NATIONAL ADVISORY COMMITTEE FOR AERONAUTICS

TECHNICAL NOTE 3847

FATIGUE-CRACK-PROPAGATION AND RESIDUAL-STATIC-STRENGTH RESULTS ON FULL-SCALE TRANSPORT-AIRPLANE WINGS

By Richard E. Whaley, M. J. McGuigan, Jr.,
and D. F. Bryan

Langley Aeronautical Laboratory
Langley Field, Va.

Washington
December 1956

NATIONAL ADVISORY COMMITTEE FOR AERONAUTICS

TECHNICAL NOTE 3847

FATIGUE-CRACK-PROPAGATION AND RESIDUAL-STATIC-STRENGTH RESULTS ON FULL-SCALE TRANSPORT-AIRPLANE WINGS

By Richard E. Whaley, M. J. McGuigan, Jr., and D. F. Bryan

SUMMARY

Results are presented of fatigue-crack-propagation studies conducted during fatigue tests of nine complete wings from C-46 airplanes. Also presented are the results of static tests of these wings with fatigue failures of various extents.

In general the cracks grew at a slow, fairly uniform rate during a large portion of the fatigue life until a certain critical percentage of the structure had failed, after which the cracks grew rapidly. This critical percentage was found to vary inversely with the load level. The portion of the fatigue life during which the crack was present and growing also varied in the same manner.

Another constant-level test on one outer panel with a machined notch in the 30-percent-chord spar also produced a propagation curve similar in shape to all the other propagation curves.

The static tests of partially failed wings indicated that the strength of the tension surface was considerably less than the calculated strength obtained from consideration of the amount of material that failed. In spite of this strength reduction in the tension surface, the resistance of the wing to the bending loads to be expected in flight was very good even with large failures present. This condition occurred because, in order to have adequate strength for the negative design load, the lower surface had excess strength for the positive design load.

The reduction in strength of the tension surface varied with the amount of material failed and was independent of the particular elements involved in the area that failed in fatigue. This strength reduction was found to compare favorably with the results of similar tests on small monoblock specimens.

INTRODUCTION

There appears to be little doubt that the practical and economically feasible aircraft structure will suffer some sort of fatigue difficulties

before its useful life has been completed. Fortunately, in the majority of past cases, these difficulties have not caused catastrophic failure of the structure. Those cases which have encountered fatigue without the subsequent loss of the airplane exhibit certain characteristics in various degrees. These characteristics are (1) slow fatigue-crack propagation, particularly through the basic structure, which enables the detection of fatigue during inspections of the airplane, and (2) no serious loss in static strength before the discovery of the fatigue crack. Not all airplanes have possessed these favorable fatigue characteristics. Thus the question arises as to why some aircraft structures possess these favorable characteristics whereas others do not. This question can not be answered completely at this time, but some information which bears directly on this question has been obtained as a result of a fatigue research program on the wings of C-46 airplanes.

The purpose of this paper is to examine the C-46 wing structure in some detail in its relation to crack propagation and residual static strength. The propagation of all fatigue cracks is shown accompanied by an explanation of the progress of the crack through the elements of the structure. Some of the reasons for the particular behavior observed are discussed. The actual static strength of the wings is compared with the calculated strength. The basic information is summarized in tabular form, shown graphically, and compared, where possible, with other similar test data.

SPECIMENS AND PROCEDURE

The general characteristics of the C-46 airplane are listed in reference 1. Each specimen consisted of a center section and two outer panels. The wing structure was of the all-metal, riveted, stressed-skin type of construction. A cross section of the wing structure at wing-span station 214, where most of the fatigue cracks occurred, is shown in figure 1. The wing skin, doubler plates, and hat-section stiffeners were made of 2024-T3 aluminum clad material and the spar caps and all other stiffeners were 2024-T4 aluminum extrusions.

All the fatigue cracks occurred on the tension surface of the wing. The tension surface of the wing is defined as all structural material below the original neutral axis of the wing with the exception of the shear webs of the spars. The details of the tension surface of the wing in the area of interest are shown in figure 2 in which all structural elements of skin, doublers, spar caps, and stiffeners have been assigned an identification number. The size and a description of each of these elements is included in table I. Also shown in figure 2 is a plan view of a portion of the tension surface of the outer panel showing the location of the various skin areas with respect to the span stations.

It can be seen from table I and figure 2 that the heavy tee stiffener, element 30, is the largest single element in the tension surface and is one of the principal members of the structure in resistance to wing bending loads. This large stiffener forms the flange of a third wing spar about 3 inches inboard of station 195, where the outer panel joins the center section.

Some pertinent characteristics of the structure at span station 214 are given in the following table:

Total tension area, sq in.	11.927
Percentage of tension area in skin and doublers	58.4
Percentage of tension area in spar caps	11.2
Percentage of tension area in stiffeners	30.4
Moment of inertia of complete wing section, for positive bending loads, in.^{4}	4057.81

Constant-amplitude-type fatigue tests were conducted on nine complete wings at five different alternating-load levels Δn of 1.00, 0.625, 0.425, 0.35, 0.25, and all were superimposed upon a mean load of 1.00g. The design ultimate load factor was 4.63 in combination with an airplane gross weight of 45,000 pounds. Two specimens (complete wings) were tested at the highest load, three at the next highest, two at the next, and one at each of the two lowest loads. Most of the constant-amplitude tests are described in reference 1 and a photograph of the constant-amplitude fatigue-testing setup is shown as figure 3.

In order to force a crack to originate in a heavy element or a spar cap, rather than in the skin, one other outer panel was slightly modified. One of the rivets which attached the wing skin to the tension spar flange near span station 210 was removed and a sharp (0.001-inch radius) notch was machined into the side of the hole through the flange. This wing was tested at a constant amplitude of 0.625g.

In almost all cases, the fatigue cracks in the wing structure were discovered when they were about $\frac{1}{4}$ inch long, or less. The chordwise projected length of all cracks was measured for all calculations. The discovery of these small cracks was made possible by the use of bonded wires as crack detectors supplemented by careful and frequent visual inspections. The use of these bonded wires to detect small fatigue cracks is described in appendix A of reference 1. Once a crack was discovered, a detailed record of its growth was kept, and each measurement was correlated with the number of cycles of load applied. The accurate measurement of the cracks was very difficult in some cases because the stiffeners and some doubler plates were inside the wing. Measurements of these internal elements were accomplished through several inspection cutouts at this wing station with the aid of a mirror. The fatigue cracks

were allowed to grow to different extents on the various specimens and ranged from a rather small crack up to ones which included about one-half the cross-sectional area of the tension surface. In some of the later tests, the wings were inspected periodically with a portable X-ray machine in addition to the visual inspections.

After the fatigue tests were completed, the outer wing panels were removed from the wing center section and placed in the static testing fixture which is shown in figure 4. The outer wing panels were then loaded by means of hydraulic jacks until complete failure of the structure occurred.

RESULTS AND DISCUSSION

Fatigue-Crack Propagation

General description of cracks.- All the fatigue cracks that grew until their respective propagation curves indicated that the wing would fail if the test were continued are listed in table II. The cracks occurred at three different locations which are indicated in figure 2 and can be described generally as follows:

Area	Location	Span station
I	Vicinity of cutout B	214
II	Corner of cutout F	214
III	Joggle in doubler	195

Of the 17 cracks reported here, 12 originated in area I, 3 in area II, 1 in area III, and 1 in a machined notch. Nine of the 12 cracks that originated in area I initiated at the edge of the external doubler plate between the 30-percent-chord spar and cutout B. The other three initiated only a few inches away at the outboard rear corner of cutout B. A small crack sometimes originated in the doubler (element 11) in the forward inboard corner of cutout B. This crack never grew until another crack originating in area I progressed to it so both were considered to be in area I. All these cracks progressed through the same elements in approximately the same order.

For purposes of the crack-propagation studies, the linear measurements of the cracks were converted to cross-sectional area and expressed as a percentage of the total original cross-sectional area of the tension surface of the wing at the span station at which the crack occurred.

The individual crack-propagation curves for all the cracks and explanations of the sequence of material that failed are shown in figure 5. The region shown in these figures is where all fatigue activity occurred. This region is from cutout A to cutout F as shown in figure 2. In most instances the number of cycles for complete failure of the wing could be estimated with reasonable accuracy because of the steep slope of the propagation curves at the cessation of fatigue tests. The point, near the end of the test, at which the propagation changes from slow growth to rapid growth is defined as the critical point. This point was determined by the intersection of two straight lines faired through the initial-low-slope portion and the final-high-slope portion and is indicated by an × on the propagation curves that have a critical point. A few fatigue cracks were not allowed to grow beyond the critical point in order to have wings with small amounts of material failed for the residual-static-strength tests. In these cases the number of cycles to complete failure of the wing could not be estimated.

Constant-amplitude tests.- All cracks originated at some stress-raiser. In most cases the cracks initiated in the skin or doubler and grew at a uniform rate until a stiffener was encountered. The stiffener then usually slowed the progress of the crack in the skin while the stiffener itself failed progressively. The rate of crack growth through the stiffener was, in most cases, more rapid than the preceding skin failure as indicated by the discontinuities in the initial-low-slope portion of some of the propagation curves. Most of the skin and doublers in the neighborhood of a stiffener were failed before the stiffener itself failed completely so that, when the stiffener did fail, the load it formerly carried was shifted directly to another stiffener or spar. The best example of this action is shown (see fig. 5(p)) by the failure of the bulb tee (element 29). After it failed, the load was transferred to the heavy tee and the 30-percent-chord spar flange (elements 28 and 30) because the neighboring skin and doubler (elements 3 and 13) had already failed. This situation resulted in a slow rate of crack propagation until a crack initiated in the adjacent heavy stiffeners (element 28 or 30). The stiffener failures will be discussed later.

No large stiffeners or spar caps (elements 28 and 30) were failed completely before the critical point was reached. In most cases the failure of one of these elements was involved in the increase in rate of growth at the critical point. In some cases, such as the curves of figures 5(b) and 5(l), a definite critical point was reached and the crack growth became rapid before the crack started in either element 28 or 30. Thus, a definite critical point is not due to the location of the initial crack in relation to these heavy elements.

In figure 6 the propagation curves of typical failures for several load levels are shown. The abscissa in this figure is the number of load cycles applied expressed as a percentage of the number of cycles

to complete wing failure as estimated from the propagation curves of figure 5. It can be seen from figure 6 that the critical point usually occurred at about 95 percent of the total lifetime and the percentage of cross-sectional tension area failed at the critical point decreased as the load level increased. This latter trend is shown graphically in figure 7 in which the percentage of tension area failed at the critical point is shown as a function of the load level. This figure indicates that, at some constant load level higher than those used in these tests, the critical percentage of area failed would be so small that all the observable crack growth would probably be beyond the critical point and thus very rapid. There is scatter in the data especially at the intermediate level of $\Delta n = 0.625$. This spread is caused partially by the fact that more specimens were tested at this level than any other level and because cracks initiated in all three failure areas at this level. The spread is also caused by the fact that some curves did not possess a sharp knee and thus the critical point was subject to some variation.

Figure 8 shows the relation between the load level and the percentage of lifetime remaining after a crack has attained a size of 1 percent of the cross-sectional tension area. This figure indicates that the percentage of the lifetime remaining after this small crack size has been attained decreases with increasing load level. Some of the scatter present in this figure is probably caused by the difficulty in determining the lifetime at the 1-percent-failure point since the propagation curves are very nearly horizontal in this region. These data points should not be expected to fall along a smooth curve since the structure is a complex one composed of many elements. The same areas are not involved in all the wings at the 1-percent-failure point.

In view of the trends shown by figures 7 and 8, it appears that at higher load levels there is less lifetime remaining after the crack has initiated and the critical percentage becomes smaller. This might indicate that, for an airplane subjected principally to high loads as might be encountered in severe maneuvers, all the visible crack growth would be beyond the critical point and therefore very rapid. It is generally assumed in this country as well as in other countries that low rather than high constant loads are more representative of the gust-load spectrum of a transport airplane. If this is true then there would appear to be a considerable portion of the lifetime during which the crack would grow slowly, at least for this type of structure. This long period of slow growth would allow considerable time for the crack to be discovered during normal inspections of the airplane in service. The advantage of this favorable situation might be difficult to realize if the crack initiated in a large stiffener or spar cap that was in itself a larger portion of the tension area than the critical percentage.

Notched-spar test.- An attempt was made to investigate in more detail the effect of the location of the initial fatigue crack on the

crack-propagation characteristics. Since all the cracks thus far discussed originated either in the wing skin or doubler plates, an attempt was made to force a crack to initiate in the main (30-percent-chord) spar flange by notching it as previously described. As can be seen from the crack-propagation curve of figure 5(q), the crack originated at the root of the machined notch. The growth of the crack in the spar cap, however, was extremely slow, and before it had grown appreciably cracks originated in three other locations on the wing. Attempts were made to stop drill two of these cracks with 1/8-inch holes in order to obtain the information desired from the spar flange, but the propagation of these cracks was slowed only slightly by the stop drilling. The test was discontinued when about 15 percent of the wing tension area had been failed by the skin cracks whereas the crack in the spar still amounted to only about 7 percent of the spar-flange area. The fact that the propagation curve exhibits a gradual increase in slope in the region of the critical point could be due to the stop-drilling operations and the complicated effects of several cracks growing concurrently. The 30-percent-chord spar appears to be one of the more highly stressed elements in the structure. Since the initial cracking did start at the end of the machined notch, it was expected that the spar flange would fail completely at an early stage. This, however, was not the case. The final failure of the wing, however, occurred much sooner than any other failure at the same load level. This could have been expected if the crack in the spar flanges had progressed through the flange early in the test. The small size of the crack at the end of the test, however, should not have affected the final lifetime.

Crack propagation through stiffeners.- An attempt was made to obtain information on the fatigue-crack propagation through individual stiffeners and spar caps. Crack-propagation curves for several stiffeners and spar caps are shown in figure 9. Considerable difficulty was experienced in obtaining the data since the stiffeners and spar flanges were on the inside of the wing and could only be viewed through inspection cutouts by using a mirror and light. Propagation information was obtained only on elements 28, 29, and 30 because these elements were the only ones large enough in the principal region of fatigue activity from which propagation data could be obtained. All three of these stiffeners were tee-shaped extrusions as shown by figure 2. The first point on each stiffener propagation curve was the last observation in which no crack was observed in the stiffener. Some of these figures contain several curves. Each figure represents one specimen and may contain curves for several stiffeners on both wings.

A crack-propagation curve similar to the crack-propagation curves of the entire wing structure was obtained from the failure of one of the spar flanges (element 28). This curve is shown in figure 9(e). The element was from a wing tested at the lowest load level so that the maximum stress in the element was lower than that in any other of the wings

tested. A fatigue crack was detected by a crack detector wire (indicated by the letter E) when only about 5 percent of the element was failed. The crack then progressed to a rivet hole which slowed the progress of the crack. The curve then exhibited a critical point where the growth of the crack became rapid. This critical point occurred at about 10 percent of the area of the element, which agrees with the percentage at the critical point for the entire wing structure at this load level.

Another propagation curve similar to the propagation curves of the entire wing structure was obtained from another element. This curve is shown in figure 9(b). This element is the heavy tee stiffener (element 30). Although the load level Δn of the test was 0.625, the rate of progress of the crack was slow. One reason for this was that element 30 had a larger area than any other element in the wing and started to fail when the wing had a little more than 1 percent of the entire area failed. The most noticeable difference between this curve and the wing propagation curves was that the critical point occurred at about 35 percent of the area of the element. That point corresponded with the critical point for the whole wing at which time 5.8 percent of the wing tension area was failed. The shape of these stiffener propagation curves depends on the alternating load level and the increase in stress in the stiffener during the test. The failure of the surrounding material causes more load to be added progressively to the stiffener and thus increases the stress. Since the cracks progress through the elements in slightly different orders in each wing, the stiffener propagation curves are subject to some variation.

Residual Static Strength

General description of static failures.- After the wings had been fatigue tested until various amounts of the cross-sectional tension area had failed, most of the wings were then tested in the static-test loading fixture to determine the remaining static strength.

The stress distribution in the wing when loaded on the static-test fixture was very nearly the same as that when the outer panels were loaded while attached in the normal manner on the wing center section in the fatigue testing machine. The chordwise stress distribution is shown in figure 10 for a loading of 4.0g which is applied in both loading devices. The station chosen for this survey (station 235) was the closest station to the area of interest which was free of cutouts, doublers, and other discontinuities. It may be seen from this figure that the chordwise location of the points of maximum stress agrees well with each other and that the difference between the curves obtained from the two loading systems is small. Also included in this figure for comparison is the chordwise distribution of design bending stresses obtained from the structural analysis of the airplane.

A photograph of a typical static failure is shown in figure 11. The static failures of the C-46 wings were in general continuations of the fatigue failure already present. The failures usually ran forward from the fatigued area to the foremost inspection cutout and then slanted inboard to the leading-edge attach angle. The leading-edge structure usually failed by shear failure of the rivets attaching the skin to the attach angle. The failure in the rearward direction ran along the line of inspection cutouts at wing station 214 and sometimes shifted outboard to the edge of the internal doubler surrounding each of these cutouts. The 70-percent-chord spar always failed by shearing rivets which attached it to the wing skin and attach angle. The 30-percent-chord spar failed in a similar manner when no fatigue failure was present in this member. There were two cases in which this spar cap fractured when no fatigue failure had been observed to be present in the spar cap. An examination of both of these fractured surfaces after the static tests, however, revealed small regions of fatigue failure which amounted to 1 to 2 percent of the spar-cap area. There were also two cases in which inspection of the heavy tee (element 30) revealed small regions of fatigue failure after the static test.

In one case, failure of the wing was precipitated by buckling of the compression surface at wing station 214. Only 3 percent of the tension surface of this wing had failed in the fatigue test, and this small amount was not enough to reduce the strength of the tension surface below that of the compression surface.

Residual-static-strength analysis.- The static strength remaining in the C-46 wings after various amounts of the tension material had been failed by fatigue is included in table III. Since the moment of inertia of the wing section is a good indication of its resistance to bending loads, the static-strength data from table III have been plotted in figure 12 against the moment of inertia remaining in the wing at the beginning of each static test. Also shown in this figure is a curve representing the calculated bending strength of the wings at the beginning of the static test. The calculated strength was obtained from a reanalysis of the wing structure. This reanalysis takes into account the reduction in section properties due to the elimination from the wing section of that tension material which had been failed in fatigue. The calculations indicated that failure of the wing would occur by buckling of the compression surface until the moment of inertia was reduced to about 3,200 inches^4. Any further reduction in the moment of inertia due to loss of more tension material should result in failure of the tension surface. Figure 12 shows that the one wing which failed in compression agrees well with the calculated value, but the failure shifts to the tension surface at a point where the moment of inertia had only been reduced to about 3,900 inches^4. The actual strength falls well below that indicated by the calculated curve. This fact indicates that the strength of

the tension surface was reduced considerably more than would be indicated simply by the removal of the material failed in fatigue.

This reduction in strength is shown clearly in figure 13 in which the static strength of the tension surface of the wing is plotted against the percent of cross-sectional tension area remaining in the wing. The solid line in figure 13 shows the relationship between the calculated strength of the tension surface and the tension area remaining after fatigue failure. The calculated strength is based on the reduced section properties of the wing after the fatigue test. Structural analysis of the wing indicated the strength of the tension surface of an undamaged wing to be about 40 percent greater than that of the compression surface for positive bending loads. The calculations indicated that if the compression surface did not buckle the strength of the tension surface would be 7.49g. This value was therefore used as the calculated static strength of an undamaged tension surface, and the actual static strengths obtained from the tests are plotted as a percentage of this figure. No static-strength reduction factor due to holes or cutouts was used in this calculation.

It can be seen in figure 13 that the actual strength is less than the calculated strength by about the same amount throughout the range of the test values. This reduction amounts to about 23 percent of the static strength of an undamaged wing. This reduction in strength can also be expressed as a static-strength reduction factor which is defined here as the ratio between the calculated strength and the actual strength at the same percentage of material remaining. This factor is calculated for each wing and is listed in table III. In figure 14 this static-strength reduction factor is plotted against the percent of tension area remaining in the wing. This figure indicates that as the amount of tension area remaining in the wing decreases the static-strength reduction factor increases. This increase is due to the static strength decreasing while the difference between the calculated strength and the actual strength remains constant. This factor can be used directly along with the calculated strength to find the actual strength.

In figure 15 the residual static strength of the wing tension surface is compared with the results of tension tests conducted on $2\frac{1}{4}$-inch-wide 2024-T3 aluminum specimens (ref. 2). It can be seen that there is remarkably good agreement between the two. Extrapolation of the results of the full-scale tests to near the region of the undamaged wing indicates that a considerable reduction in static strength of the tension surface would result from a very small fatigue crack.

Residual-static-strength results.- The detailed explanation of the structural elements failed indicates that the particular elements failed on a given wing had no significant effect on the resulting static strength;

that is, the static strength was dependent only on the amount of area involved and the test points fell approximately along a line described in figure 12 or 13, regardless of whether a large stiffener or the main spar cap was included in the area that failed. This is probably due to the fact that the structure of this wing was well distributed and might not be the case in a wing structure where the bending material was concentrated in heavy elements.

The residual static strength of the C-46 wing based on design-load considerations was very good, as indicated by figure 12, principally because of the large margins of safety in the lower surface of the wing for the positive-loading case. These large margins resulted in relatively small reduction in the bending strength of the whole wing even though the strength of the tension surface itself had been considerably reduced. The large margins of safety for the positive design load were occasioned by the fact that the lower surface of the wing was critical in the negative-loading case in which very small margins were present. In other words, in order to have adequate strength for the negative design load, the lower surface had excess strength in the positive-design-load case.

The residual-static-strength data, figure 13, indicate that the C-46 wing could withstand, without failure, a positive gust which produced a load factor equivalent to the design limit load with as much as 30 percent of the lower cross-sectional area failed in fatigue. Therefore, a considerable length of time should exist in which the crack would be large enough to be easily discovered and during this time the wing could withstand without catastrophic failure any load that the airplane would be likely to encounter.

Description of failed surfaces.- Three different types of failures occurred. These three types were (1) true fatigue failure, (2) the static type of failure, and (3) a transition type between these other two types. The true fatigue failure exhibited several identifying characteristics which were as follows: (1) slow growth of the crack (2) fractured surface normal to the principal stress in the member involved, (3) no "necking down" of the element at the fracture, (4) a smoother texture of the fractured surface, (5) concentric rings or radial marks emanating from the nucleus of the fatigue failure, and (6) some residue from fretting corrosion was frequently present. The static failure of elements was, of course, abrupt and had the following characteristics: (1) the fractured surface was along the usual 45° shear plane and a feather edge was produced at the fracture, (2) necking down of the material, (3) the texture of the fractured surface was somewhat rougher and had a duller appearance than the fatigue failure. The transition type of failure progressed at a more rapid rate than the fatigue failure. The fractured surface of the larger elements was usually normal to the principal stress, but the appearance and texture of the fractured surface were more like the texture of the static failure than that of the fatigue failure.

Generally, the failure of most of the elements started as a fatigue type and then changed to the transition type. An example of this is shown in figure 16(a). At all load levels after the critical point had been passed, the failures were mostly of the transition type (see fig. 16(b)). For comparative purposes a purely static failure is shown in figure 16(c). Most of the failures did not exhibit all of the identifying characteristics enumerated, and some would be difficult to classify if it were not known beforehand which type of failure had occurred.

CONCLUSIONS

Results have been presented of fatigue-crack-propagation and residual-static-strength studies conducted on full-scale wings from C-46 airplanes.

The fatigue cracks grew slowly during a large portion of the fatigue life until a certain critical percentage of the tension structure of the wing had been failed, after which the cracks grew rapidly. This critical percentage usually occurred at about 95 percent of the fatigue life and its value was found to vary inversely with the load level. The portion of the fatigue life during which the crack was present and growing also varied in the same manner.

Another test, in which the failure was forced to initiate in a spar flange, produced a crack-propagation curve similar to the other crack-propagation curves. All indications showed that the spar flange should fail early in the test but at the end of the test the spar flange was still not completely broken. The final failure of the wing, however, occurred much sooner than for any other wing tested at the same load level.

The residual-static-strength tests on partially failed wings indicated that the strength of the tension surface was reduced by the presence of the fatigue crack more than would be indicated from an analysis of the wing when only the amount of area that failed is taken into account. In spite of this fact, the data indicated that the wing could withstand an application of positive design limit load with as much as 30 percent of the lower cross-sectional area failed in fatigue. The reason for this result was that, in order for the wing to have adequate strength for the negative design load, the lower surface of the wing had large margins of safety for the positive design load.

The reduction in strength of the tension surface was found to compare favorably with the results of similar tests on small monoblock specimens. The actual static strength was found to be related to the amount of area

that failed in fatigue and was independent of the particular elements involved in the fatigue failure.

Langley Aeronautical Laboratory,
National Advisory Committee for Aeronautics,
Langley Field, Va., July 30, 1956.

REFERENCES

1. McGuigan, M. J., Jr., Bryan, D. F., and Whaley, R. E.: Fatigue Investigation of Full-Scale Transport-Airplane Wings - Summary of Constant-Amplitude Tests Through 1953. NACA TN 3190, 1954.

2. McEvily, Arthur J., Jr., Illg, Walter, and Hardrath, Herbert F.: Static Strength of Aluminum-Alloy Specimens Containing Fatigue Cracks. NACA TN 3816, 1956.

TABLE I

DESCRIPTION OF STRUCTURAL ELEMENTS

[See figure 2]

Element (a)	Description	Thickness, in.	Length, in.	Area, sq in.	Location
1	Skin	0.040	23.00	0.920	Forward edge of cutout A to neutral axis
2	Skin	.040	20.00	.800	Rear edge of cutout A to edge of cutout B
3	Skin	.051	10.00	.510	Forward edge of cutout B to 30-percent-chord spar
4	Skin	.051	18.00	.918	From 30-percent-chord spar to forward edge of cutout F
5	Skin	.051	11.00	.561	From rear edge of cutout F to skin splice
6	Skin	.040	3.25	.130	From skin splice to forward edge of cutout G
7	Skin	.040	12.25	.490	From rear edge of cutout G to forward edge of cutout H
8	Skin	.032	12.25	.392	From rear edge of cutout H to 70-percent-chord spar
9	Doubler	.040	2.38	.095	Forward edge of cutout A
10	Doubler	.040	2.38	.095	Rear edge of cutout A
11	Doubler	.051	5.50	.280	Attach angle doubler forward of cutout B
12	Doubler	.086	2.13	.183	Forward edge of cutout B
13	Doubler	.086	2.50	.215	Rear edge of cutout B
14	Doubler	.081	3.25	.263	Forward edge of cutout F
15	Doubler	.081	3.50	.284	Rear edge of cutout F
16	Doubler	.040	4.00	.160	Forward edge of cutout G
17	Doubler	.040	4.00	.160	Rear edge of cutout G
18	Doubler	.081	3.25	.263	Forward edge of cutout H
19	Doubler	.081	3.00	.243	Rear edge of cutout H
20	Spar cap			.400	At 70 percent chord
21	Hat stiffener	.032	5.07	.162	Between 70-percent-chord spar and cutout H
22	Hat stiffener	.032	5.07	.162	Along forward edge of cutout H
23	Hat stiffener	.040	5.07	.2024	Along rear edge of cutout G
24	Hat stiffener	.040	5.07	.2024	Along forward edge of cutout G
25	Hat stiffener	.040	5.07	.2024	Along rear edge of cutout F
26	Hat stiffener	.040	5.07	.2024	Along forward edge of cutout F
27	Hat stiffener	.040	5.07	.2024	Nine inches rearward of 30-percent-chord spar
28	Spar cap			.926	At 30 percent chord
29	Bulb-tee stiffener			.3971	Along rear edge of cutout B
30	Heavy-tee stiffener			1.140	Along forward edge of cutout B
31	Bulb-angle stiffener			.0871	First stringer forward of heavy tee
32	Bulb-angle stiffener			.0871	Second stringer forward of heavy tee
33	Bulb-angle stiffener			.0871	Along rear edge of cutout A
34	Bulb-angle stiffener			.0871	Along forward edge of cutout A
35	Bulb-tee stiffener			.2968	De-icer bulb tee
36	Bulb-angle stiffener			.1166	Leading-edge bulb angle
				11.927	Total tension area at station 214

[a]Elements 1 to 19 apply to station 214.
Elements 20 to 36 apply to stations 214 and 195.

TABLE I.- Concluded

DESCRIPTION OF STRUCTURAL ELEMENTS

Element (a)	Description	Thickness, in.	Length, in.	Area, sq in.	Location
a	Skin	0.040	47.25	1.890	From middle of heavy tee to neutral axis
b	Skin	.051	17.25	.880	From middle of heavy tee to 30-percent-chord spar
c	Skin	.051	38.00	1.938	From 30-percent-chord spar to skin splice at cutout G
d	Skin	.040	24.00	.960	From skin splice at cutout G to skin splice at cutout H
e	Skin	.032	18.25	.584	From skin splice at cutout H to 70-percent-chord spar
f	Doubler	.064	30.63	1.960	External doubler over 30-percent-chord spar and heavy tee
g	Doubler	.051	28.25	1.441	From 30-percent-chord spar to forward end
h	Doubler	.051	37.38	1.905	From 30-percent-chord spar to end of doubler at cutout G
j	Doubler	.051	23.50	1.186	From end of doubler at cutout G to end of doubler at cutout H
k	Doubler	.051	18.50	.931	From end of doubler at cutout H to 70-percent-chord spar
20 to 36				4.965	Stringers and spars
				18.640	Total tension area at station 195

[a]Elements a to k apply to station 195.
Elements 20 to 36 apply to stations 195 and 214.

TABLE II

SUMMARY OF CRACK-PROPAGATION DATA

[See figure 2]

Load level, Δn	Failure (a)	Location of failure (b)	Area	Lifetime at 1% failure, cycles	Lifetime at critical point, cycles	Estimated final failure of wing, cycles	Lifetime after 1% crack, percent	Lifetime at critical point, percent	Area failed at critical point, percent	Static test
1.00	3	Edge of external doubler plate, station 207 (L, 7)	I	88,500	(c)	-------	----	----	----	--
1.00	6	Corner of inspection cutout F, station 214 (R, 7)	II	86,000	98,000	104,000	17.3	94.2	2.5	15
1.00	12	Corner of inspection cutout F, station 214 (R, 8)	II	49,000	(d)	67,000	26.9	----	----	--
1.00	15	Edge of external doubler plate, station 207 (L, 8)	I	64,000	72,800	77,500	17.5	93.9	3.7	4
.625	3	Corner of inspection cutout F, station 214 (R, 1)	II	205,000	281,500	293,000	30.0	96.0	7.1	1
.625	4	Joggle in external doubler plate, station 195 (L, 1)	III	255,000	409,000	432,000	41.0	94.5	4.0	6
.625	12	Edge of external doubler plate, station 207 (R, 2)	I	(e)	246,000	260,000	----	94.5	8.8	14
.625	15	Edge of external doubler plate, station 207 (L, 2)	I	269,000	336,000	345,000	22.1	97.4	5.8	3
.625	31	Corner of inspection cutout B, station 214 (L, 3)	I	273,500	328,000	345,000	20.8	95.1	13.0	10

[a]Failure numbers are used in conjunction with load level.

[b]Numbers refer to the order in which wing sections were tested. Letters refer to the following: L, left wing; R, right wing; NS, notched spar.

[c]Test discontinued before critical point was reached.

[d]No definite critical point.

[e]Crack discovered after 7% failed.

TABLE II.- Concluded

SUMMARY OF CRACK-PROPAGATION DATA

[See figure 2]

Load level, Δn	Failure (a)	Location of failure (b)	Area	Lifetime at 1% failure, cycles	Lifetime at critical point, cycles	Estimated final failure of wing, cycles	Lifetime after 1% crack, percent	Lifetime at critical point, percent	Area failed at critical point, percent	Static test
0.425	5	Edge of external doubler plate, station 207 (L, 4)	I	952,000	1,192,000	1,230,000	22.6	96.9	16.3	9
.425	7	Edge of external doubler plate, station 207 (R, 4)	I	886,000	(c)	----------	-----	----	----	12
.425	9	Corner of inspection cutout B, station 214 (L, 5)	I	680,000	1,031,000	1,200,000	43.4	86.0	8.0	2
.425	10	Corner of inspection cutout B, station 214 (R, 5)	I	616,000	(c)	----------	----	----	----	5
.350	3	Edge of external doubler plate, station 207 (L, 6)	I	1,320,000	(c)	----------	-----	-----	----	--
.350	5	Edge of external doubler plate, station 207 (R, 6)	I	1,270,000	1,885,000	2,010,000	36.8	93.8	9.8	11
.250	1	Edge of external doubler plate, station 207 (L, 9)	I	2,660,000	4,025,000	4,240,000	37.3	95.0	10.2	8
.625	1	Notch in 30-percent-chord spar, station 207 (R, NS)		130,000	149,000	173,000	23.5	86.1	3.2	13

[a]Failure numbers are used in conjunction with load level.

[b]Numbers refer to the order in which wing sections were tested. Letters refer to the following: L, left wing; R, right wing; NS, notched spar.

[c]Test discontinued before critical point was reached.

[d]No definite critical point.

[e]Crack discovered after 7% failed.

TABLE III

SUMMARY OF RESIDUAL-STATIC-STRENGTH DATA

Static test	Tension area remaining, percent	Moment of inertia, station 214, $in.^4$	Calculated compression strength, g units	Calculated tension strength, g units	Actual strength, g units	Static-strength reduction factor
Undamaged	100.0	4106	4.91	7.49	----	----
1	46.4	2247	4.06	2.87	1.67	1.72
2	79.9	3597	4.87	5.77	3.95	1.46
3	67.4	3159	4.56	4.67	3.10	1.51
4	84.2	3686	4.87	6.11	4.40	1.38
5	87.8	3799	4.88	6.46	4.70	1.38
6	56.8	(a)	----	----	2.25	----
7	97.4	4042	4.89	7.27	5.07	(b)
8	72.8	3342	4.75	5.37	3.60	1.49
9	57.6	2855	4.64	4.00	2.25	1.78
10	76.0	3465	4.83	5.44	3.55	1.53
11	65.8	3103	4.68	4.71	3.08	1.53
12	88.8	3832	4.90	6.55	4.84	1.36
13	84.8	3708	4.80	6.20	4.08	1.52
14	68.7	3204	4.70	5.02	2.75	1.82
15	74.0	3384	4.75	5.37	3.40	1.58

[a]Station 195 failure.

[b]Compression failure.

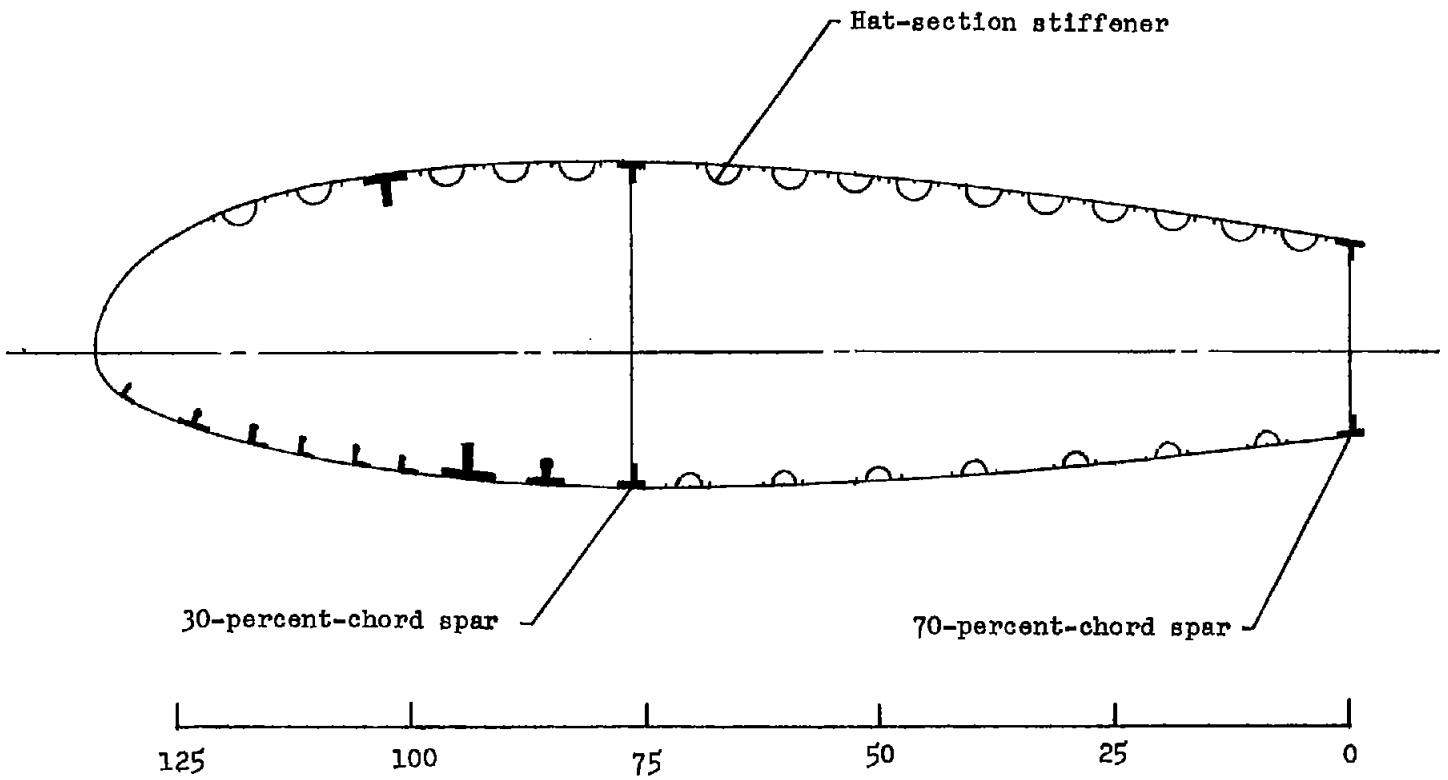

Figure 1.- General arrangement of section of outer panel at station 214.

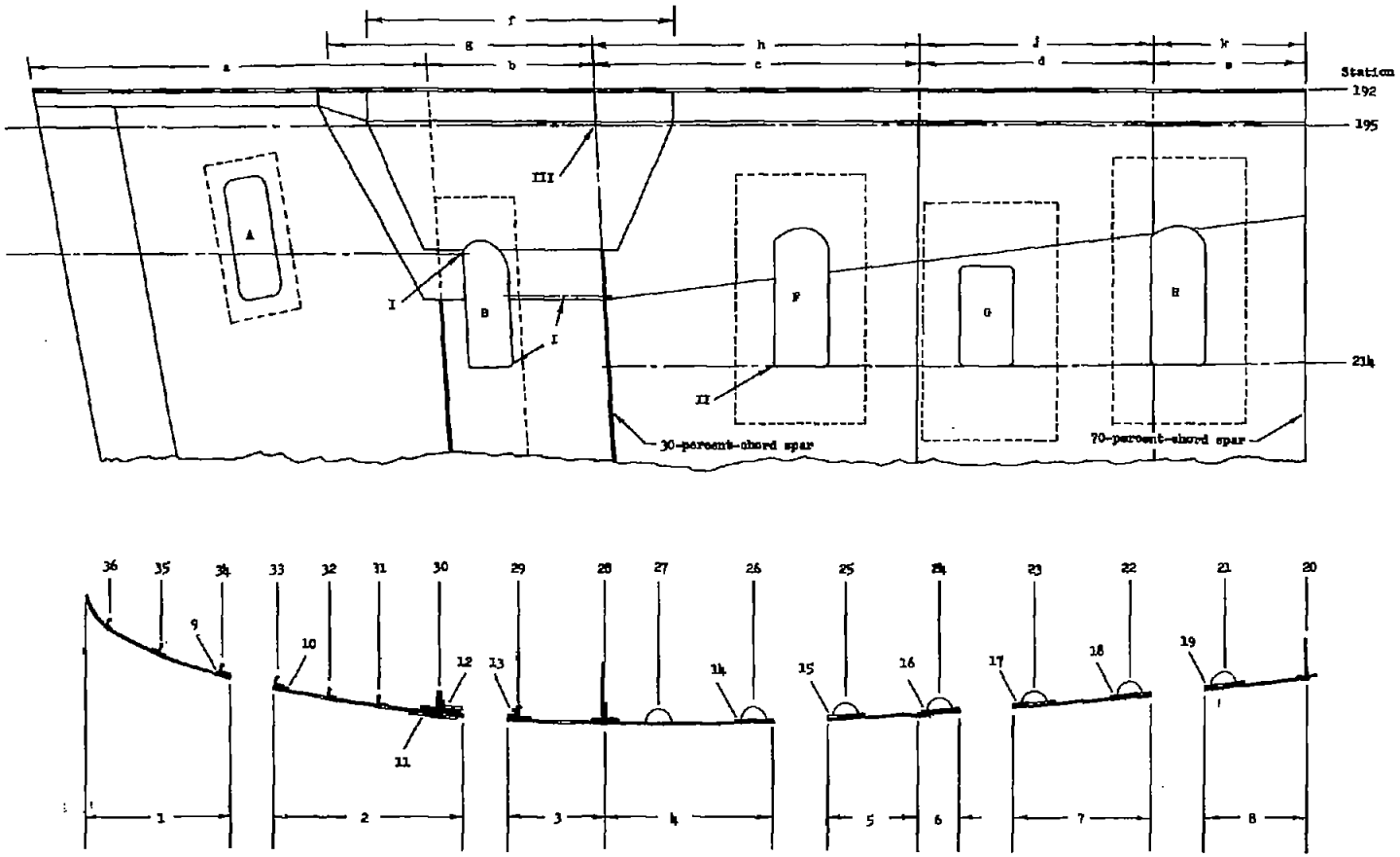

Elements 1 to 8 apply to skin at span station 214.
Elements 9 to 19 apply to doublers at span station 214.
Elements 20 to 36 apply to stiffeners at all stations.
Elements a to e apply to skin at span station 195.
Elements f to k apply to doublers at span station 195.
I, II, and III apply to the three failure areas.

Figure 2.- Details of wing structure and location of failures.

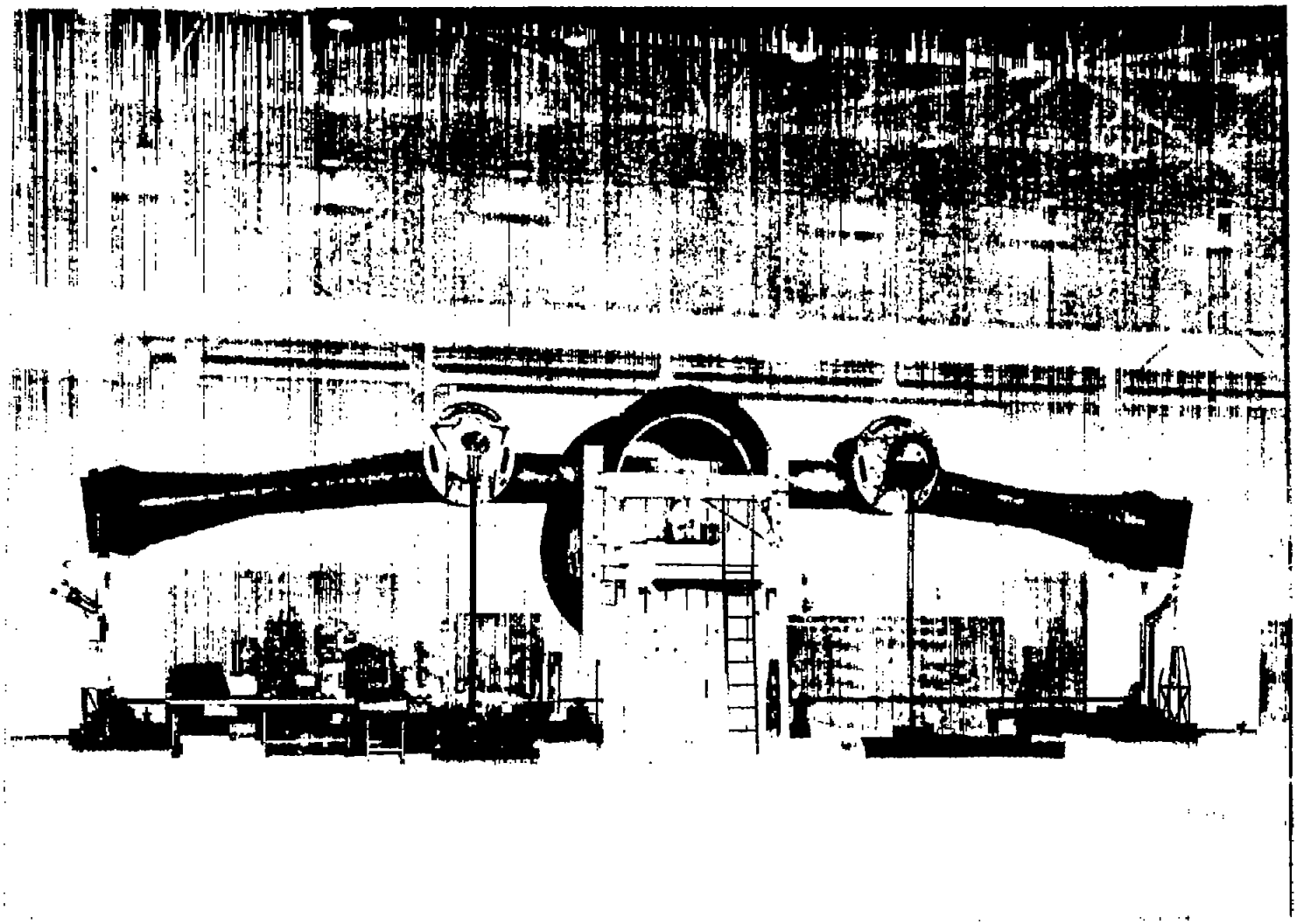

L-80028.1

Figure 3.- General view of wing mounted for test in fatigue machine.

L-89285.1

Figure 4.- General view of wing mounted for test in static testing fixture.

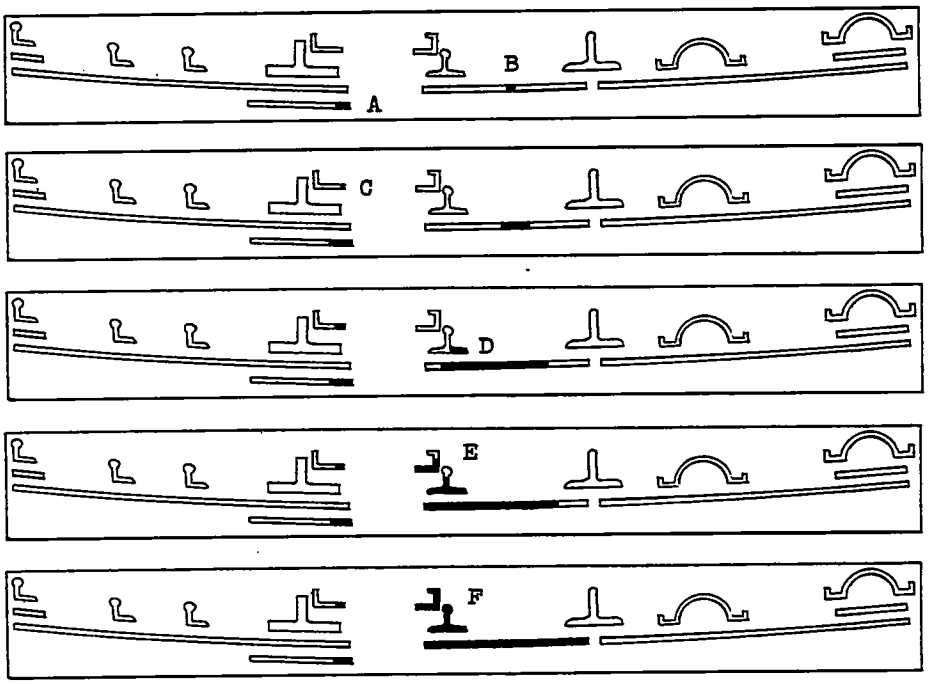

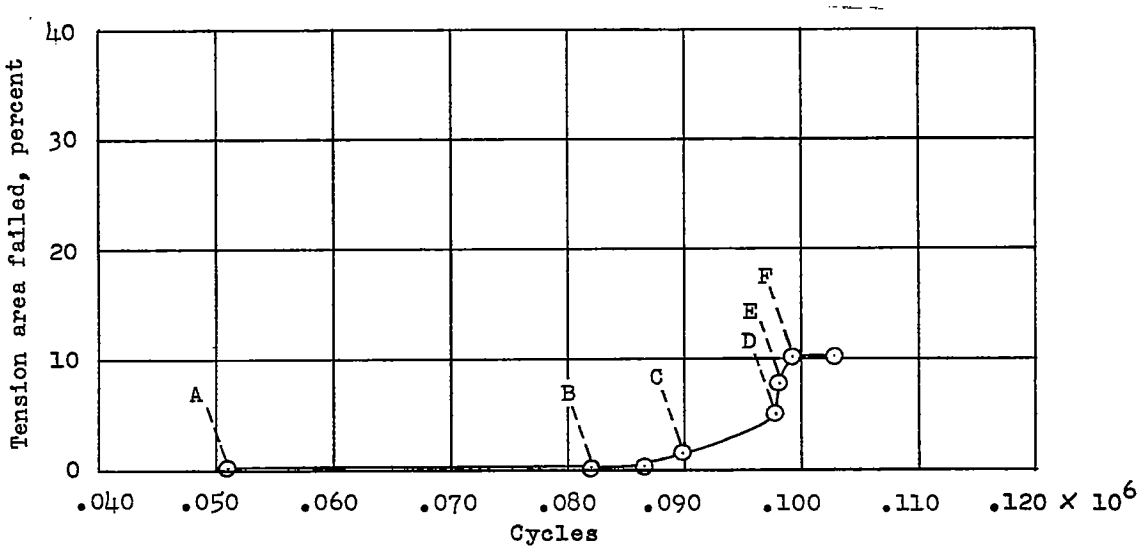

(a) Failure 3; $\Delta n = 1.00$.

Figure 5.- Crack propagation through wings.

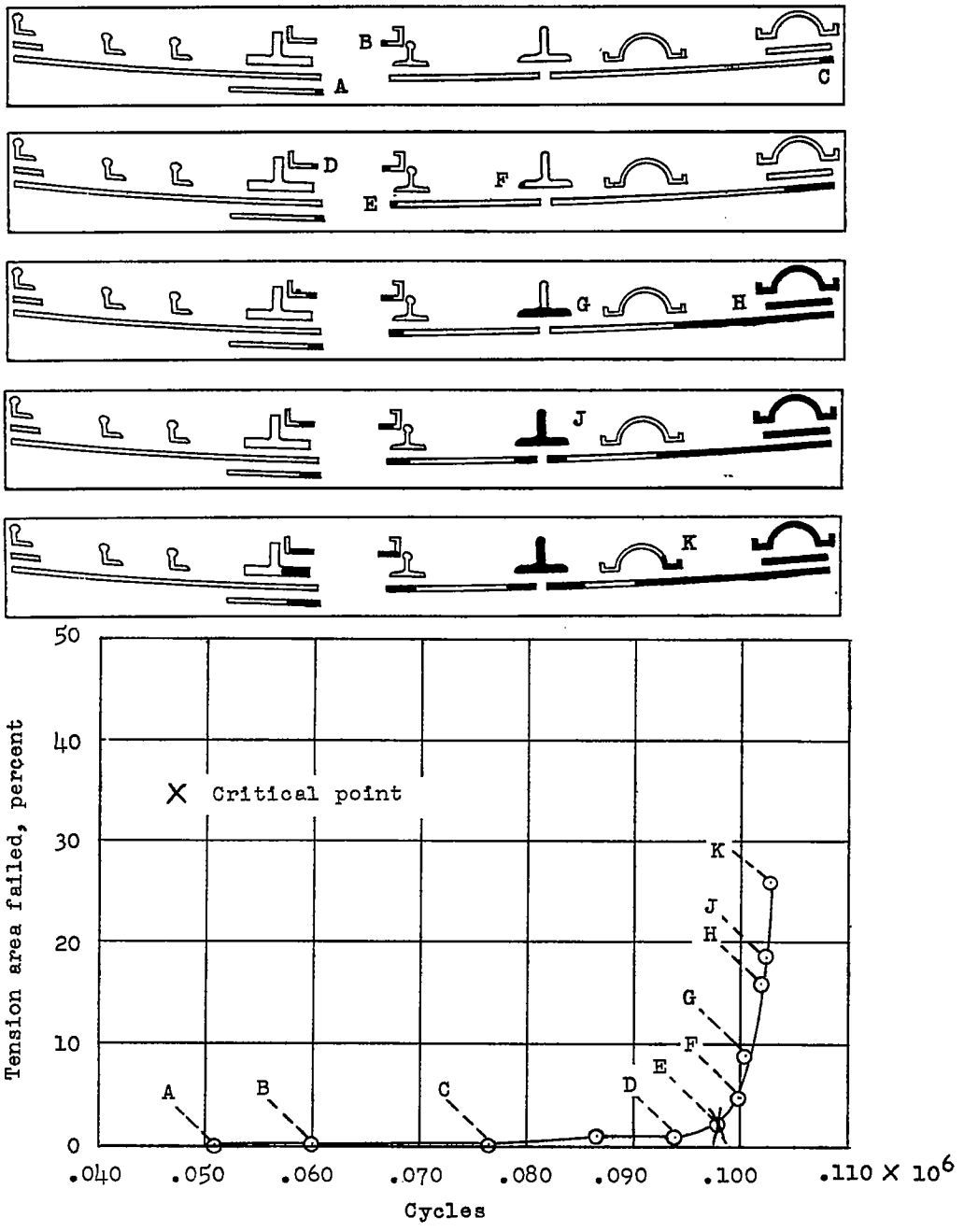

(b) Failure 6; $\Delta n = 1.00$.

Figure 5.- Continued.

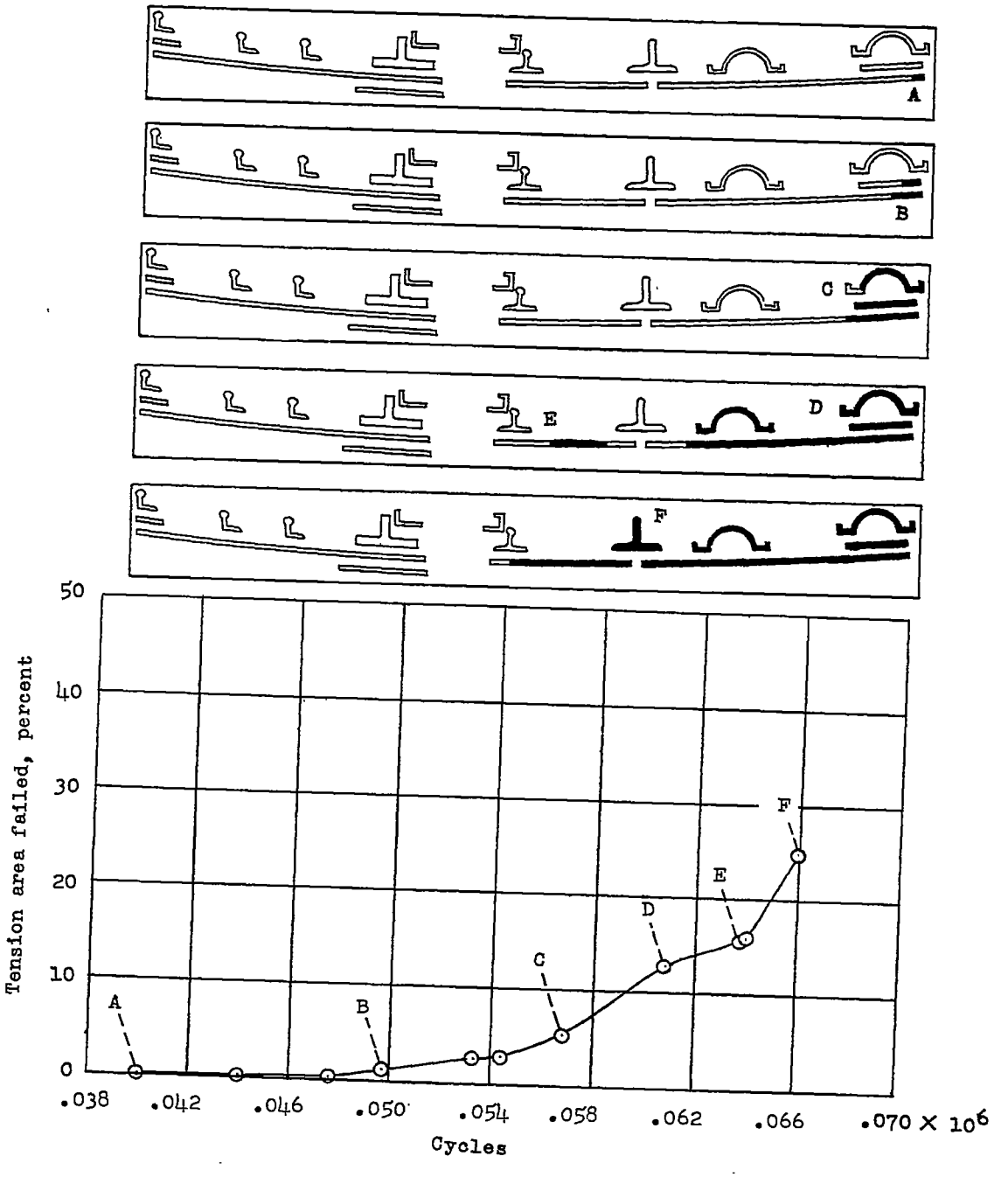

(c) Failure 12; $\Delta n = 1.00$.

Figure 5.- Continued.

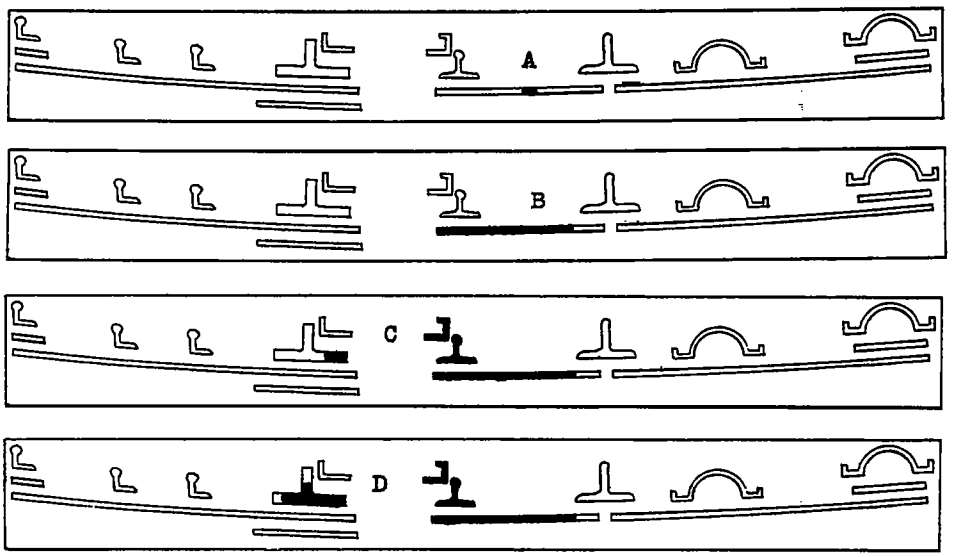

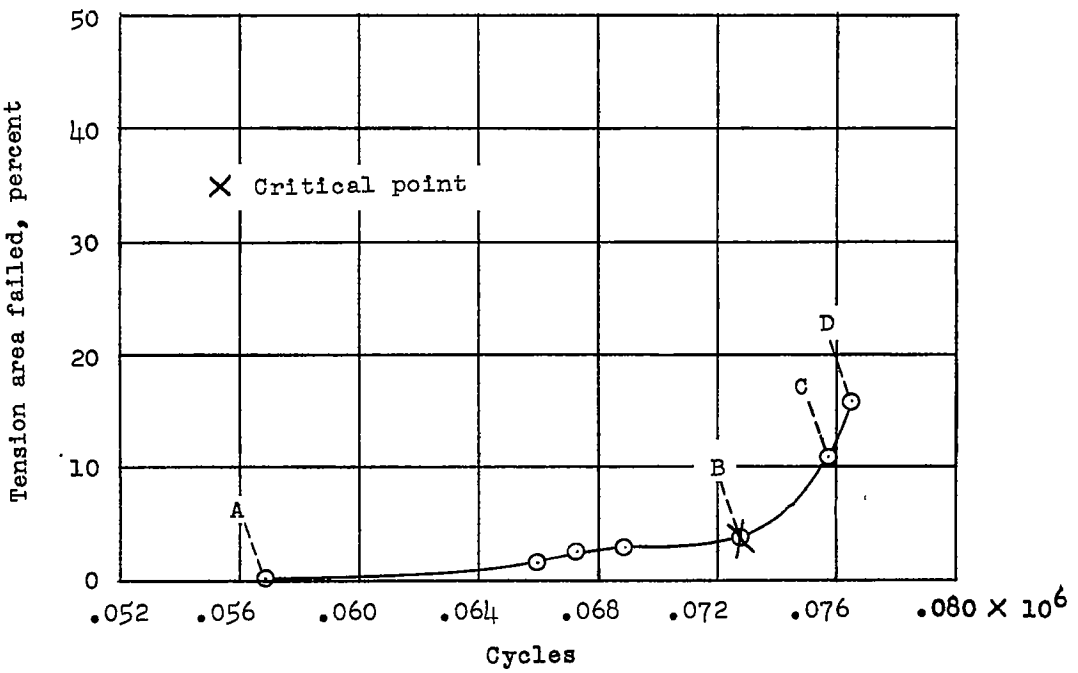

(d) Failure 15; $\Delta n = 1.00$.

Figure 5.- Continued.

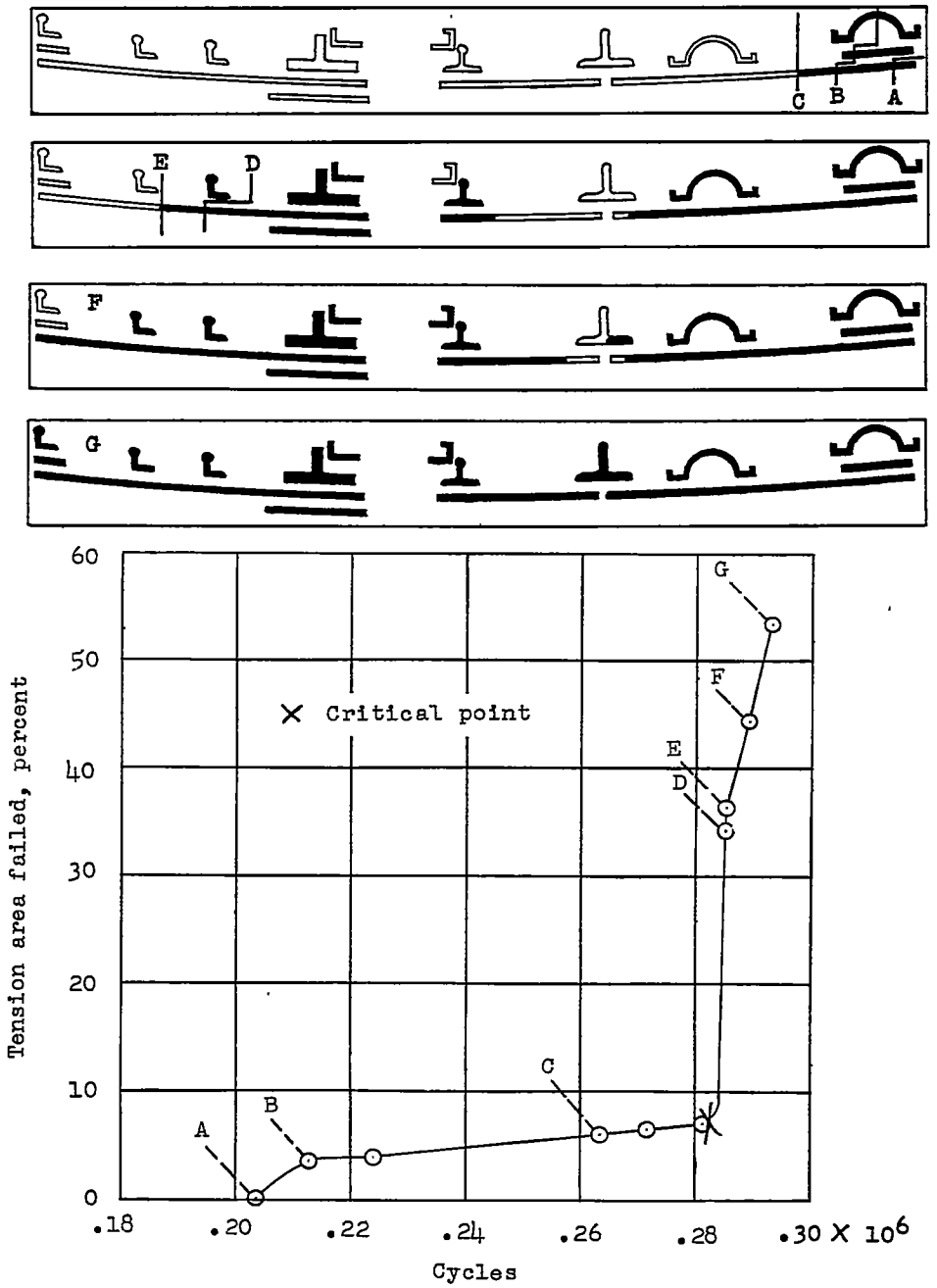

(e) Failure 3; $\Delta n = 0.625$.

Figure 5.- Continued.

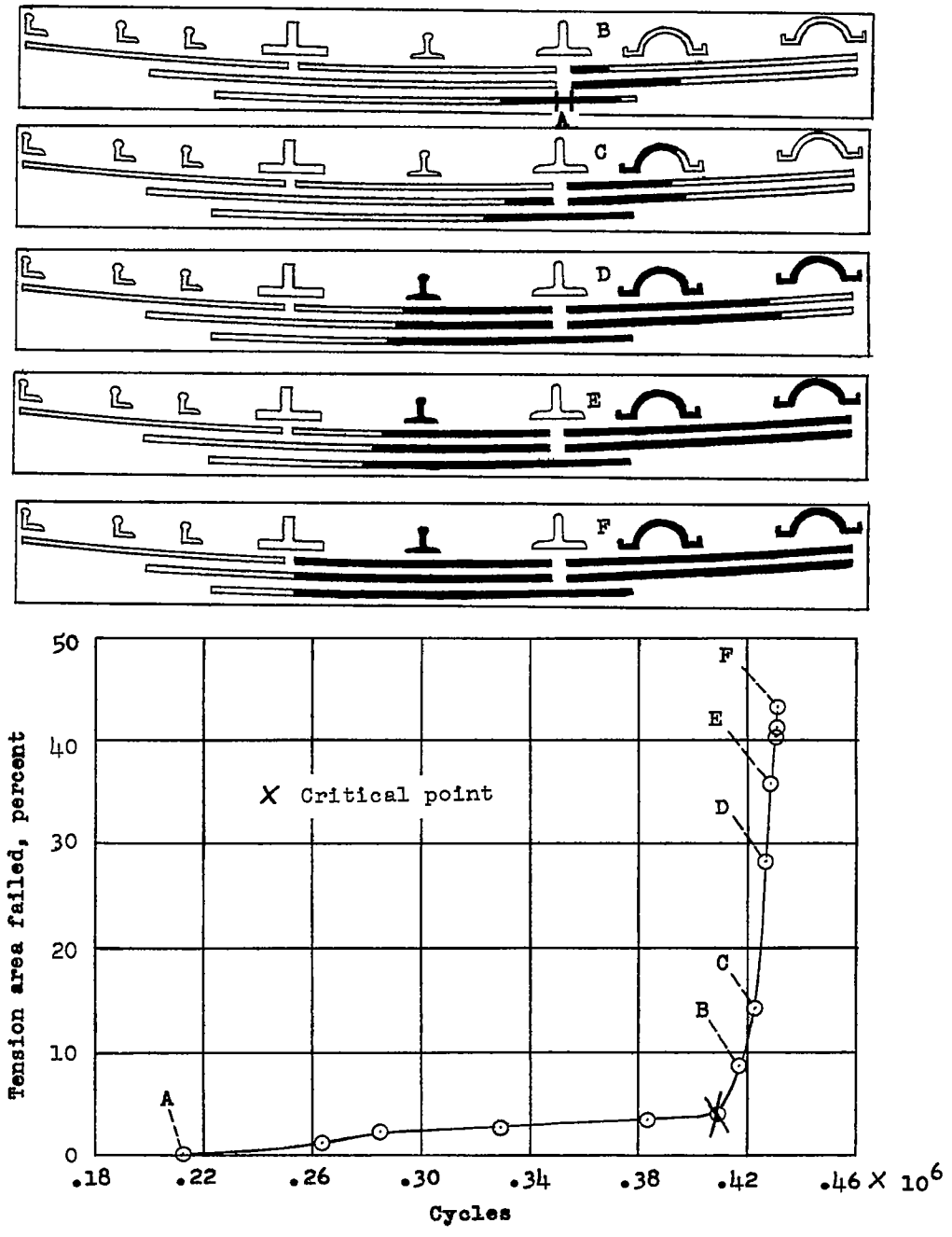

(f) Failure 4; $\Delta n = 0.625$.

Figure 5.- Continued.

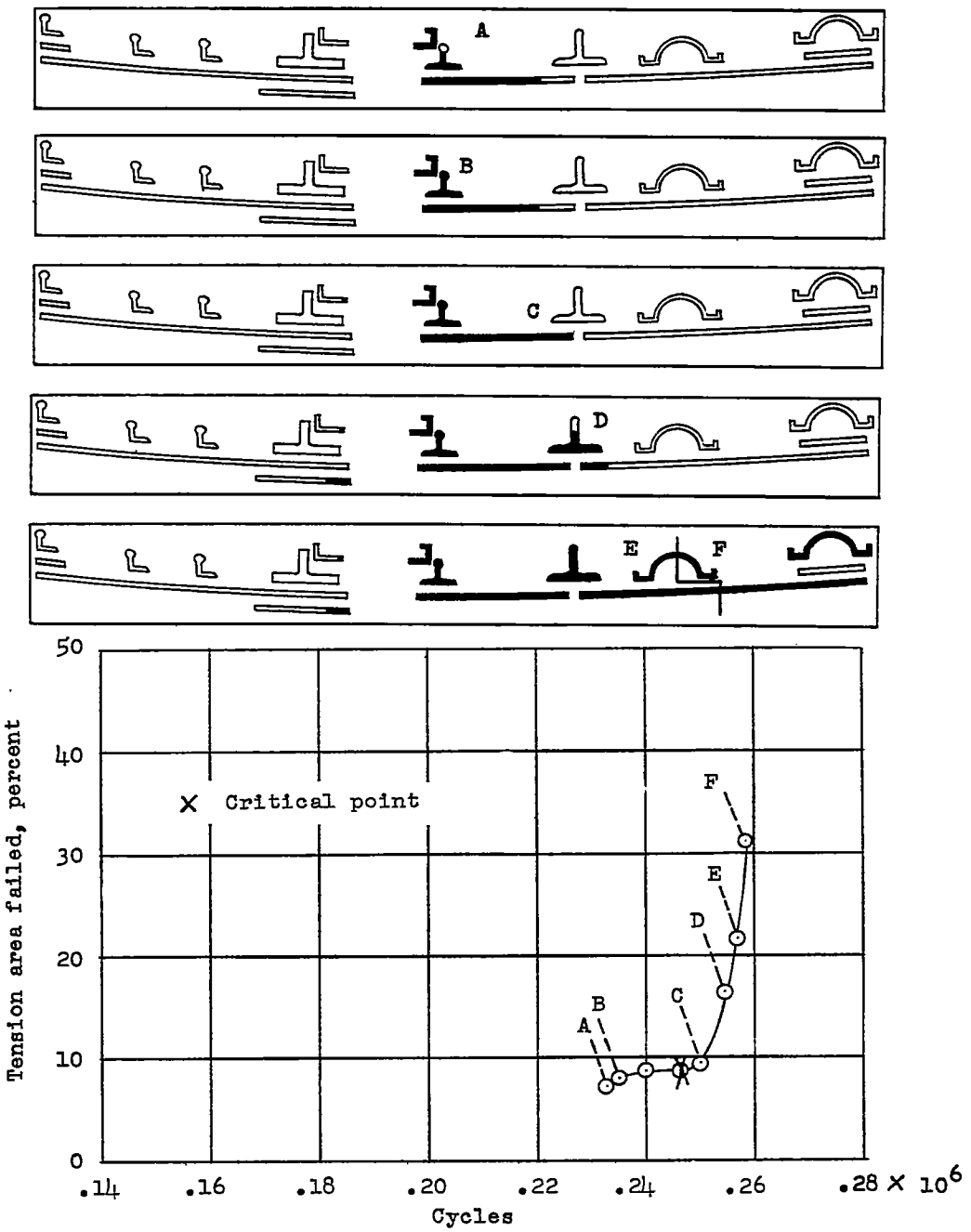

(g) Failure 12; $\Delta n = 0.625$.

Figure 5.- Continued.

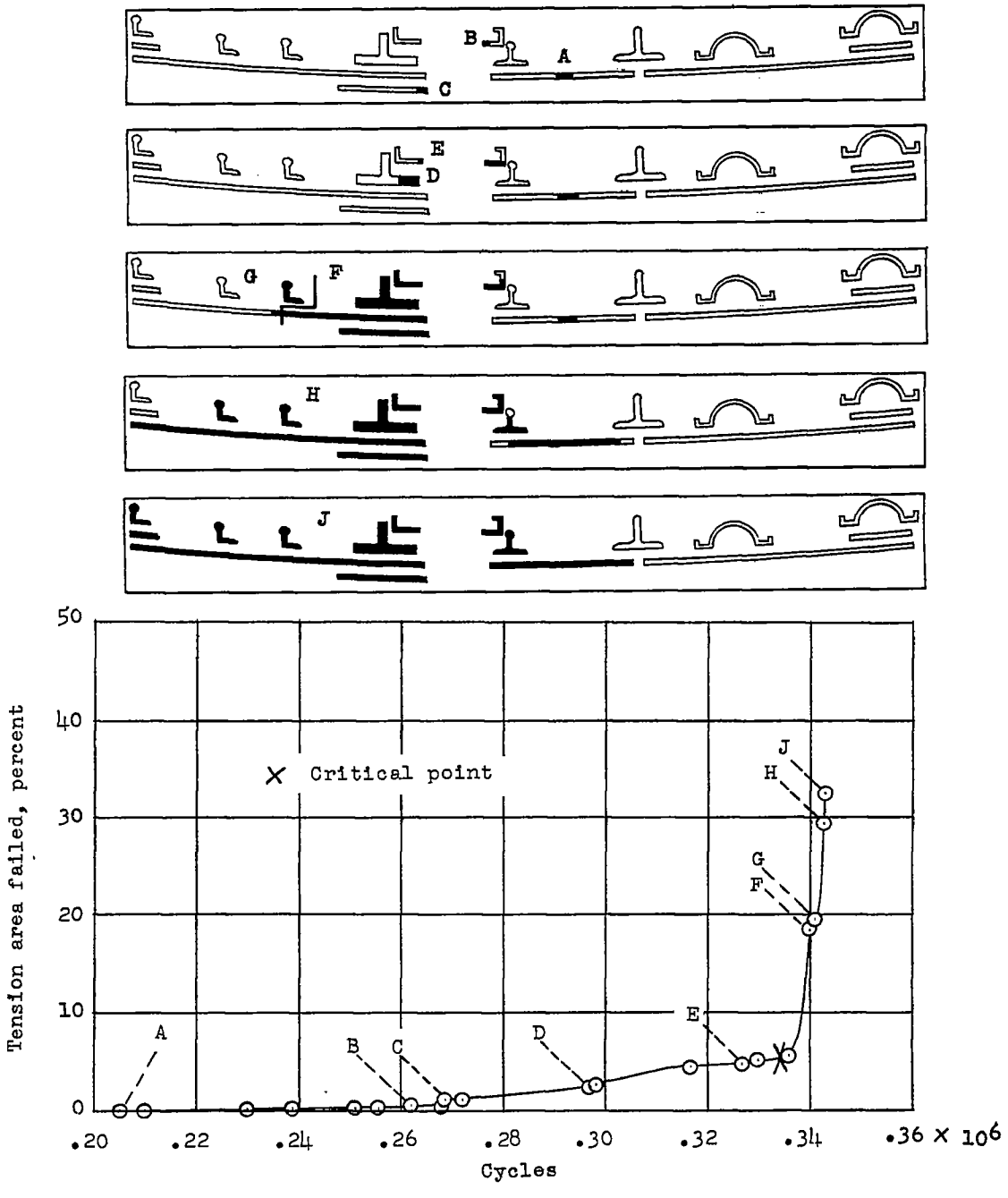

(h) Failure 15; $\Delta n = 0.625$.

Figure 5.- Continued.

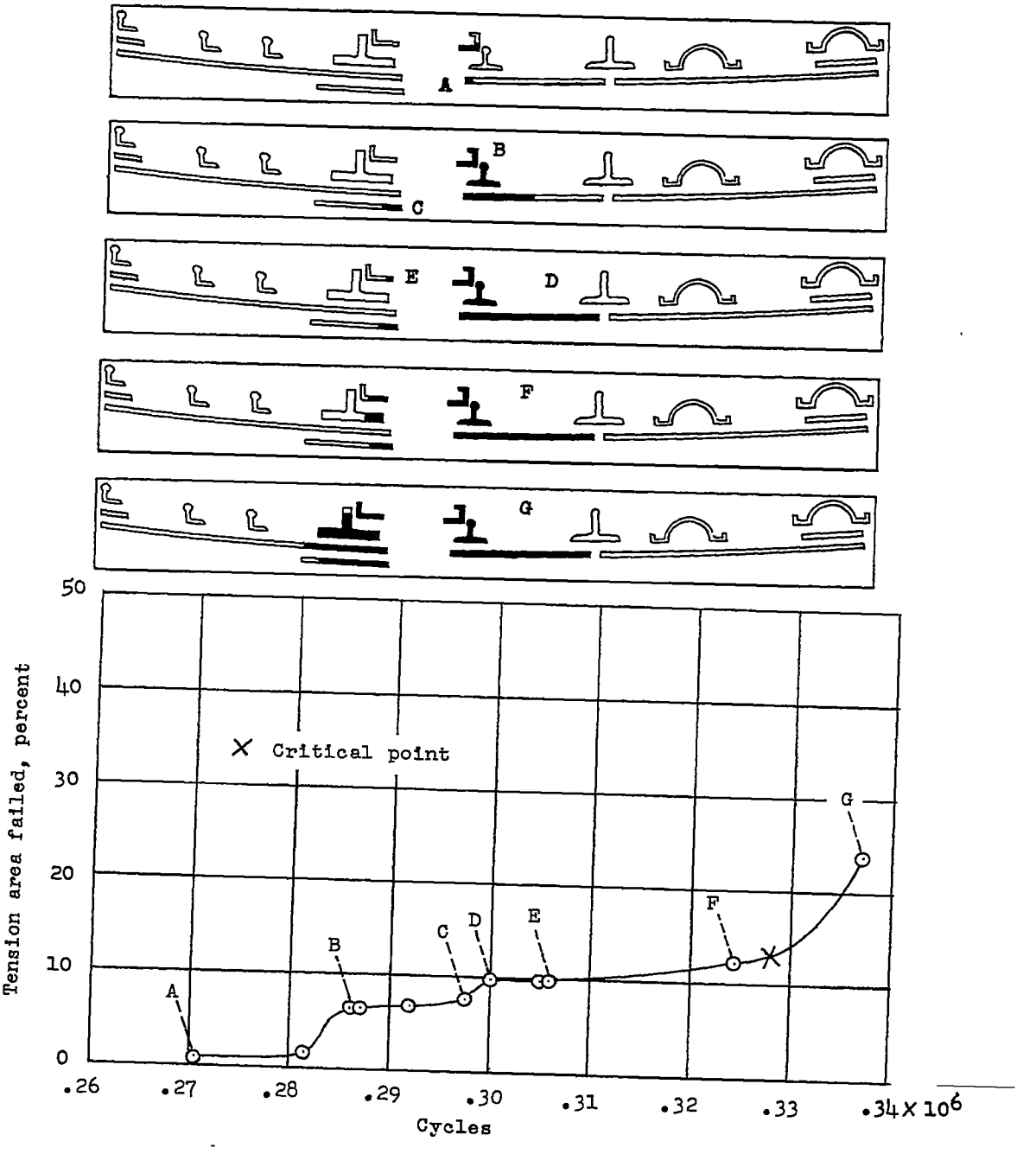

(i) Failure 31; $\Delta n = 0.625$.

Figure 5.- Continued.

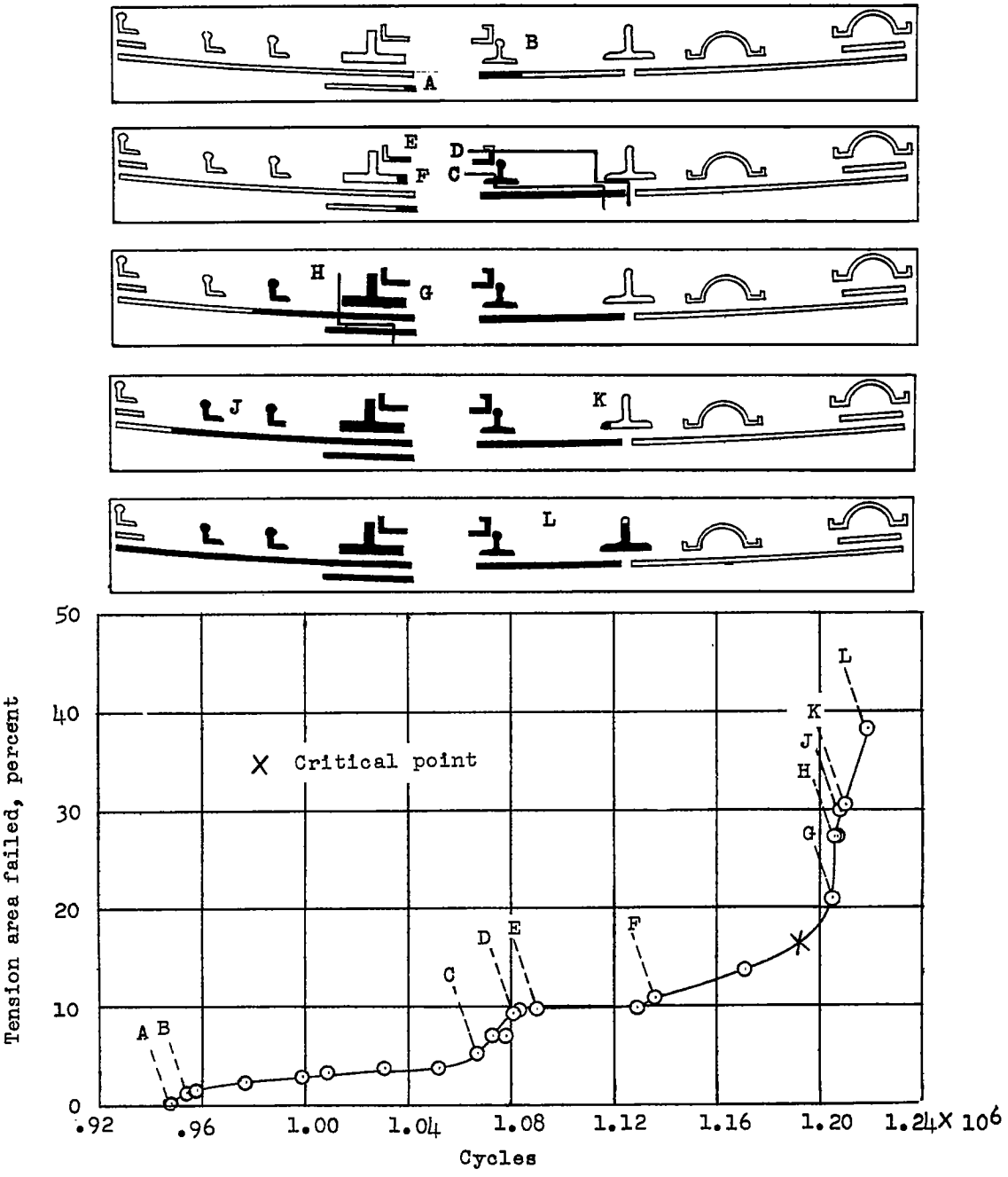

(j) Failure 5; $\Delta n = 0.425$.

Figure 5.- Continued.

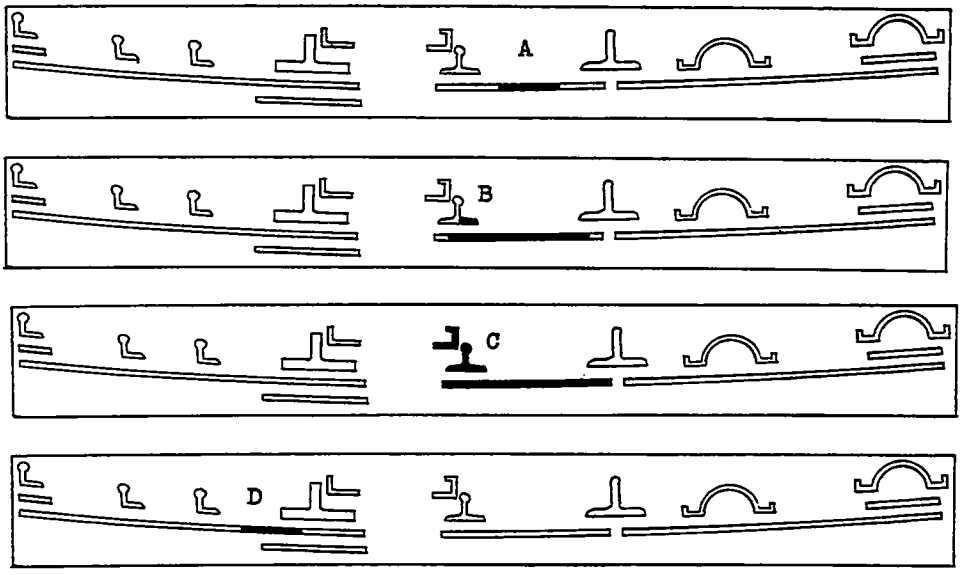

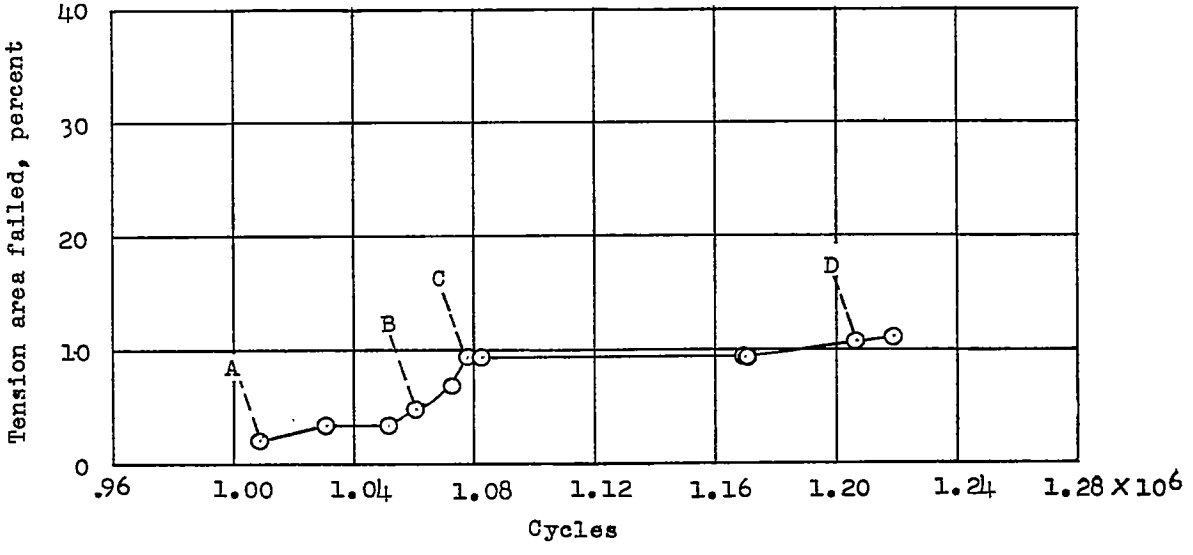

(k) Failure 7; $\Delta n = 0.425$.

Figure 5.- Continued.

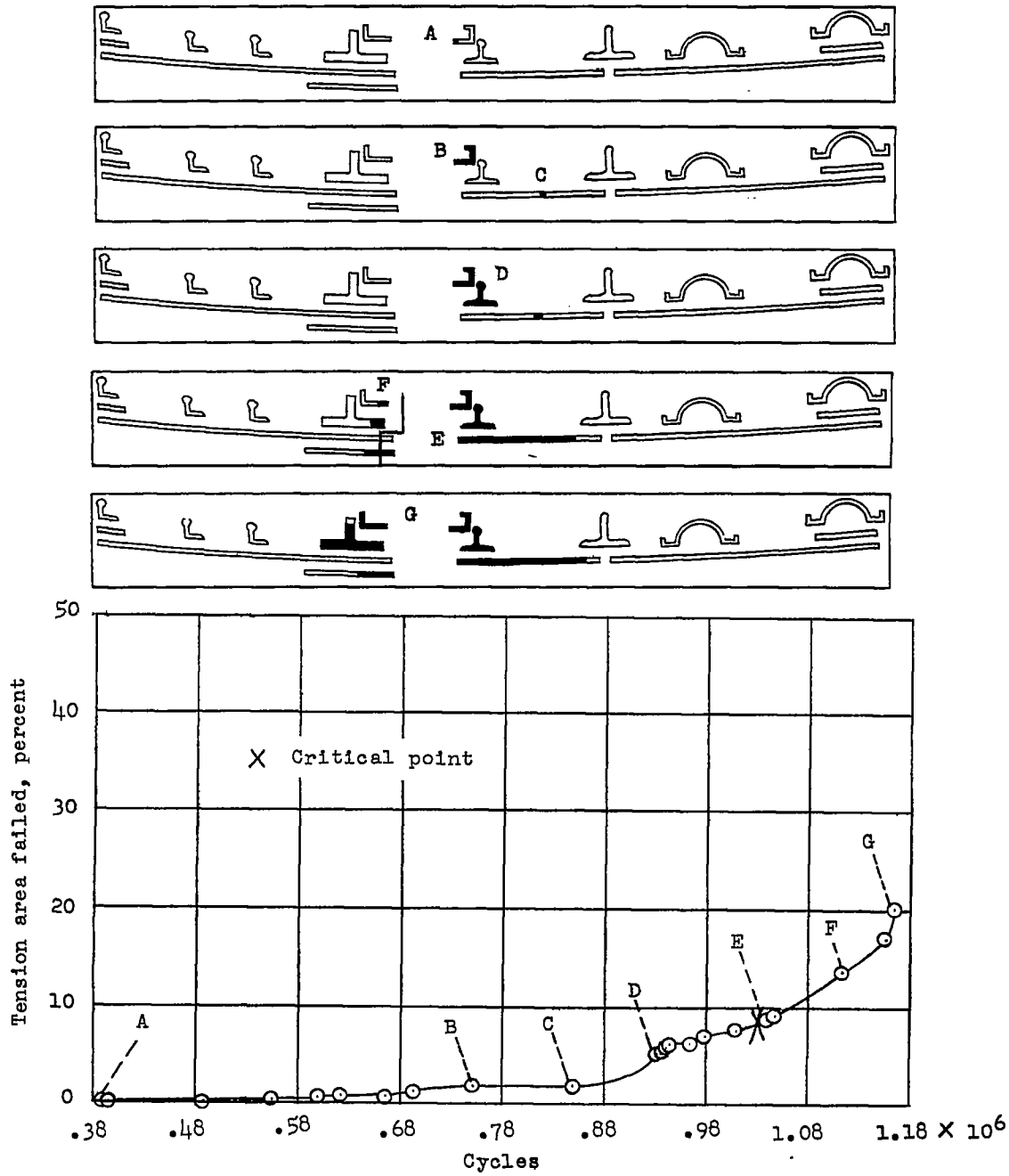

(l) Failure 9; $\Delta n = 0.425$.

Figure 5.- Continued.

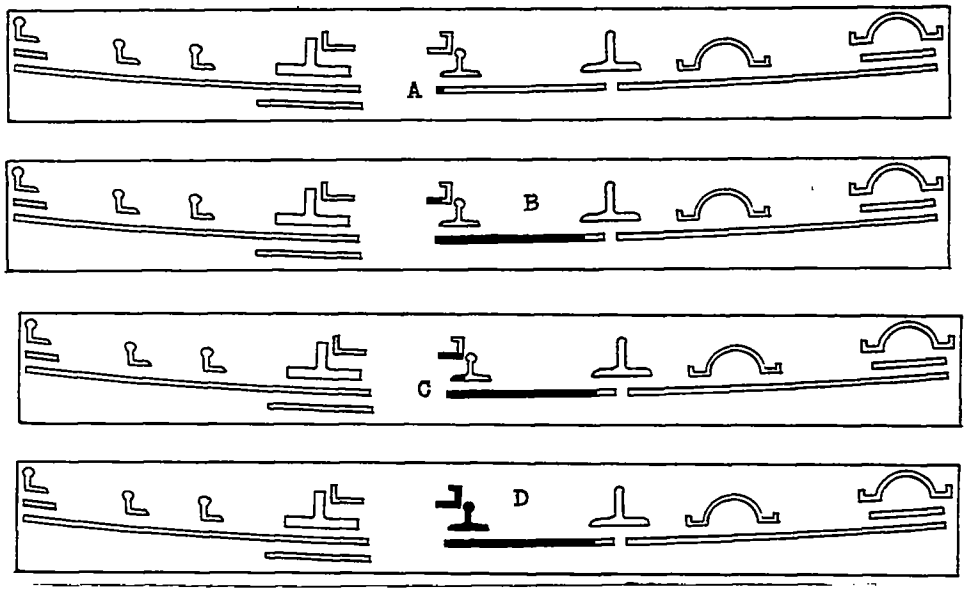

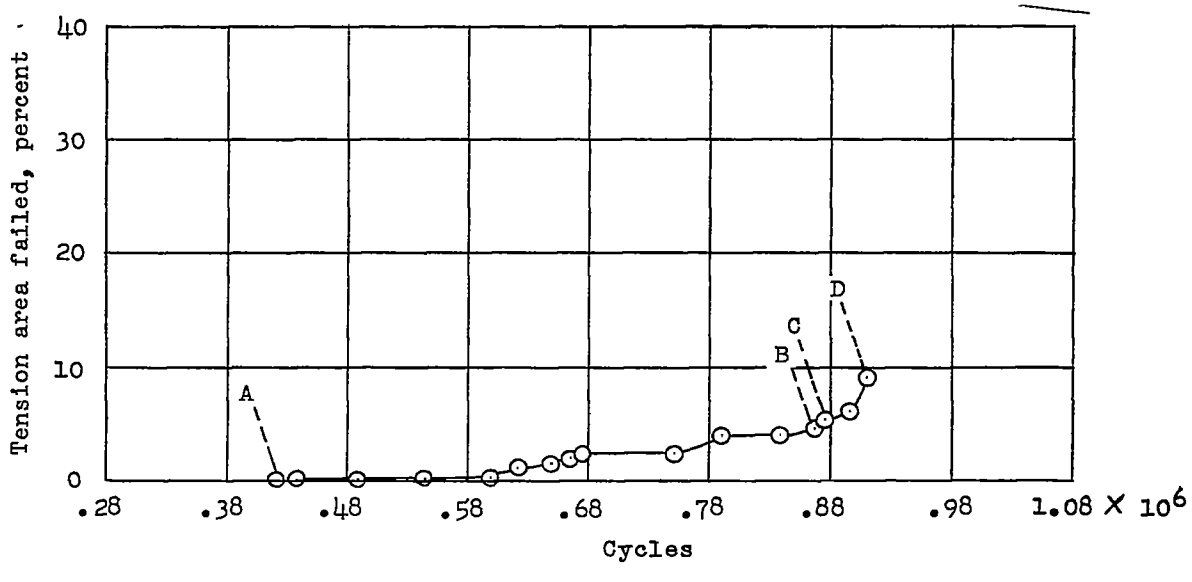

(m) Failure 10; $\Delta n = 0.425$.

Figure 5.- Continued.

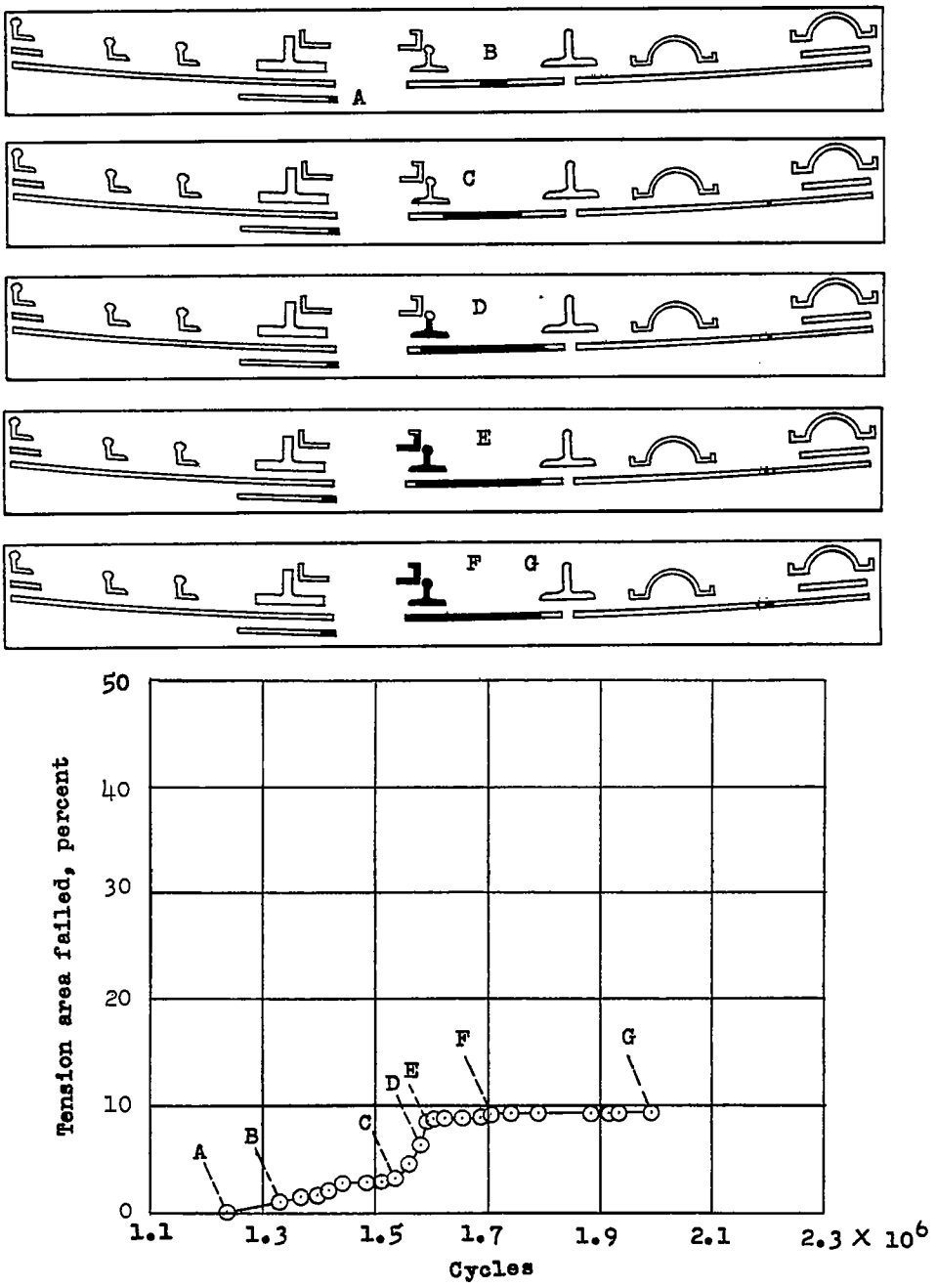

(n) Failure 3; $\Delta n = 0.350$.

Figure 5.- Continued.

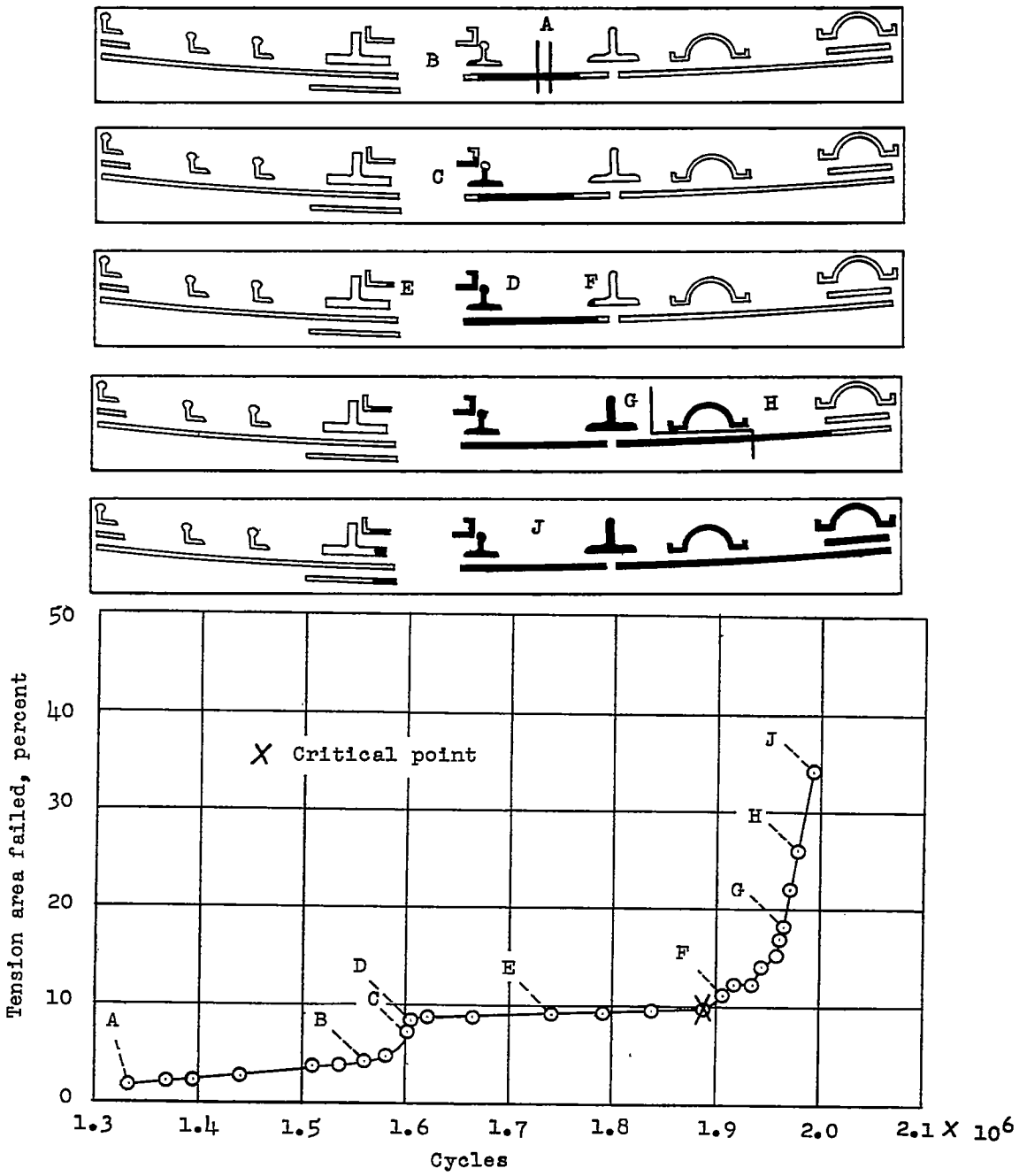

(o) Failure 5; $\Delta n = 0.350$.

Figure 5.- Continued.

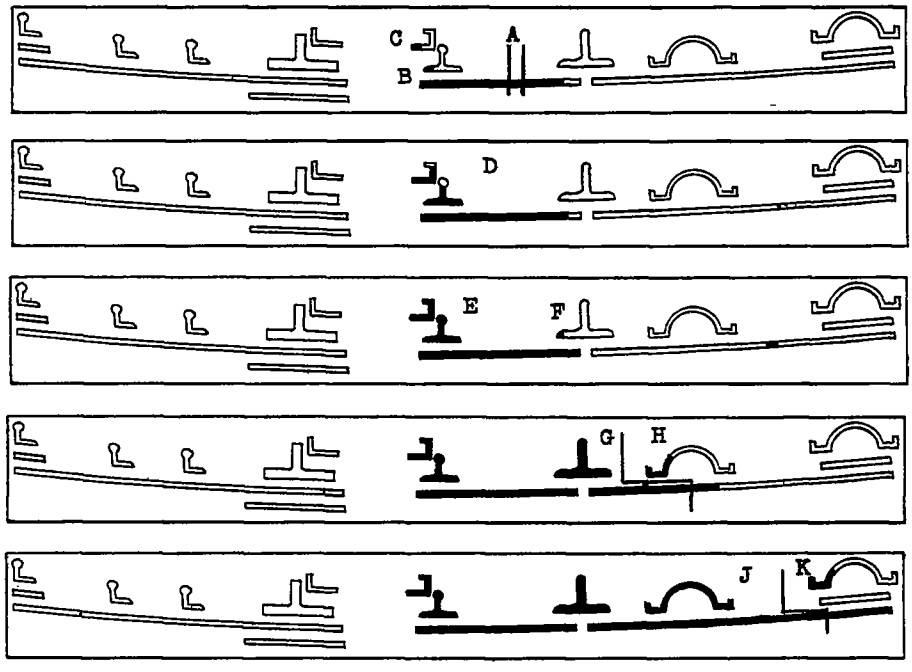

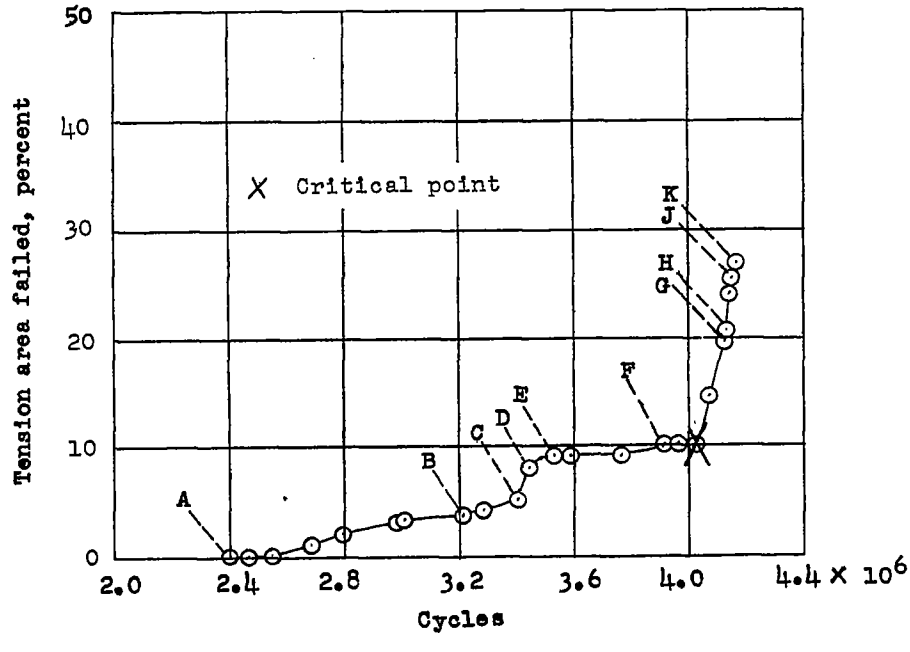

(p) Failure 1; $\Delta n = 0.250$.

Figure 5.- Continued.

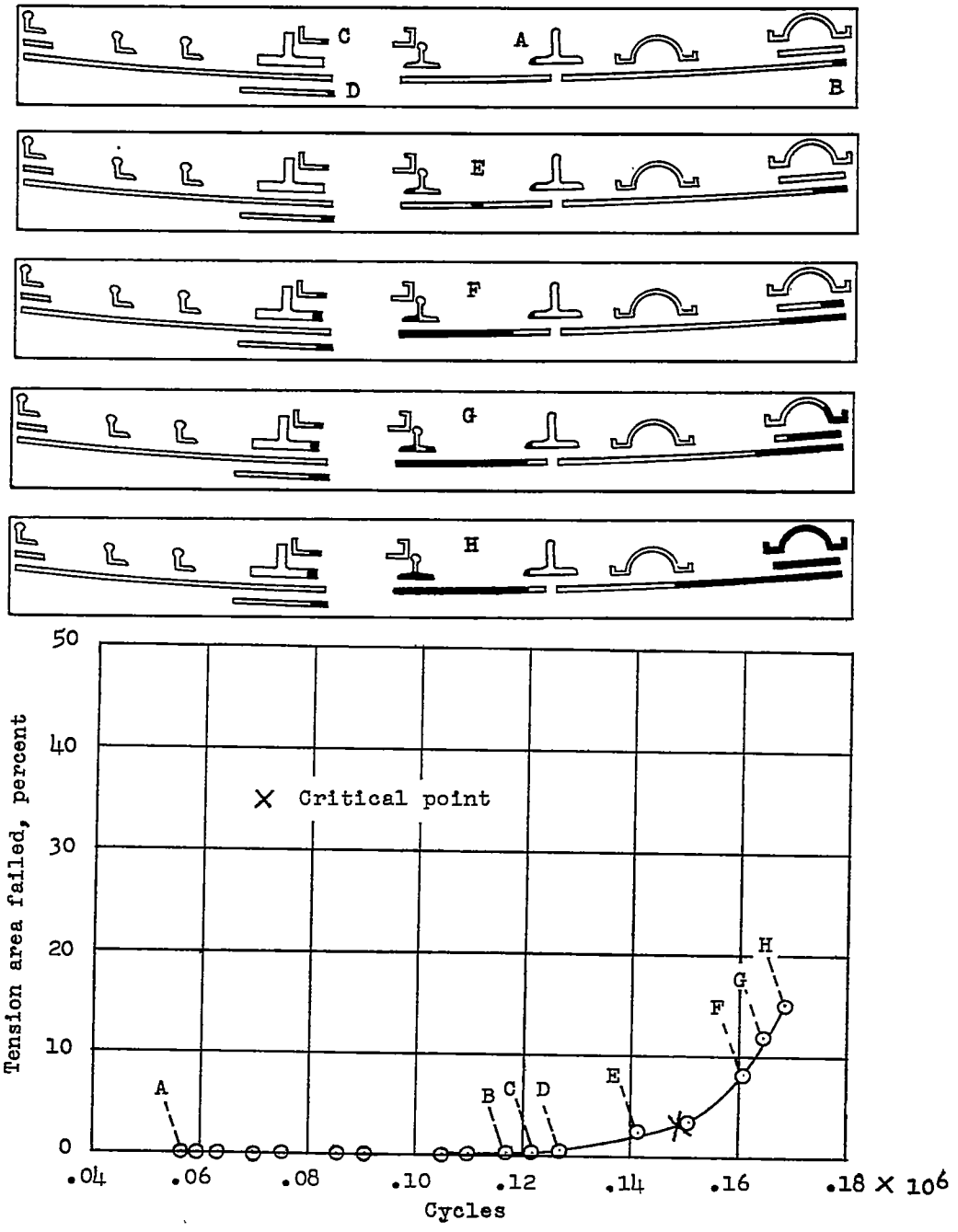

(q) Crack 1; notched spar; $\Delta n = 0.625$.

Figure 5.- Concluded.

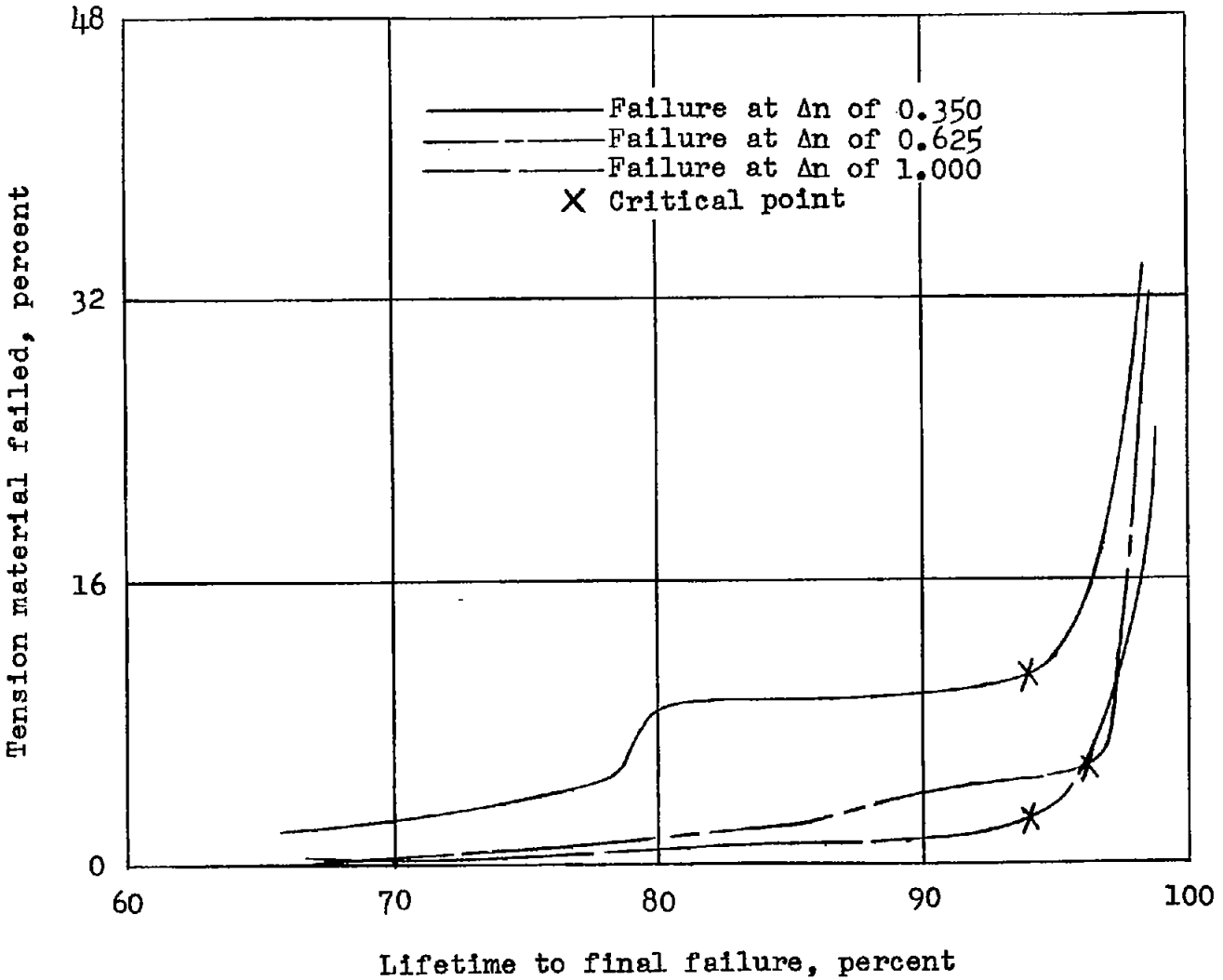

Figure 6.- Typical fatigue-crack propagation.

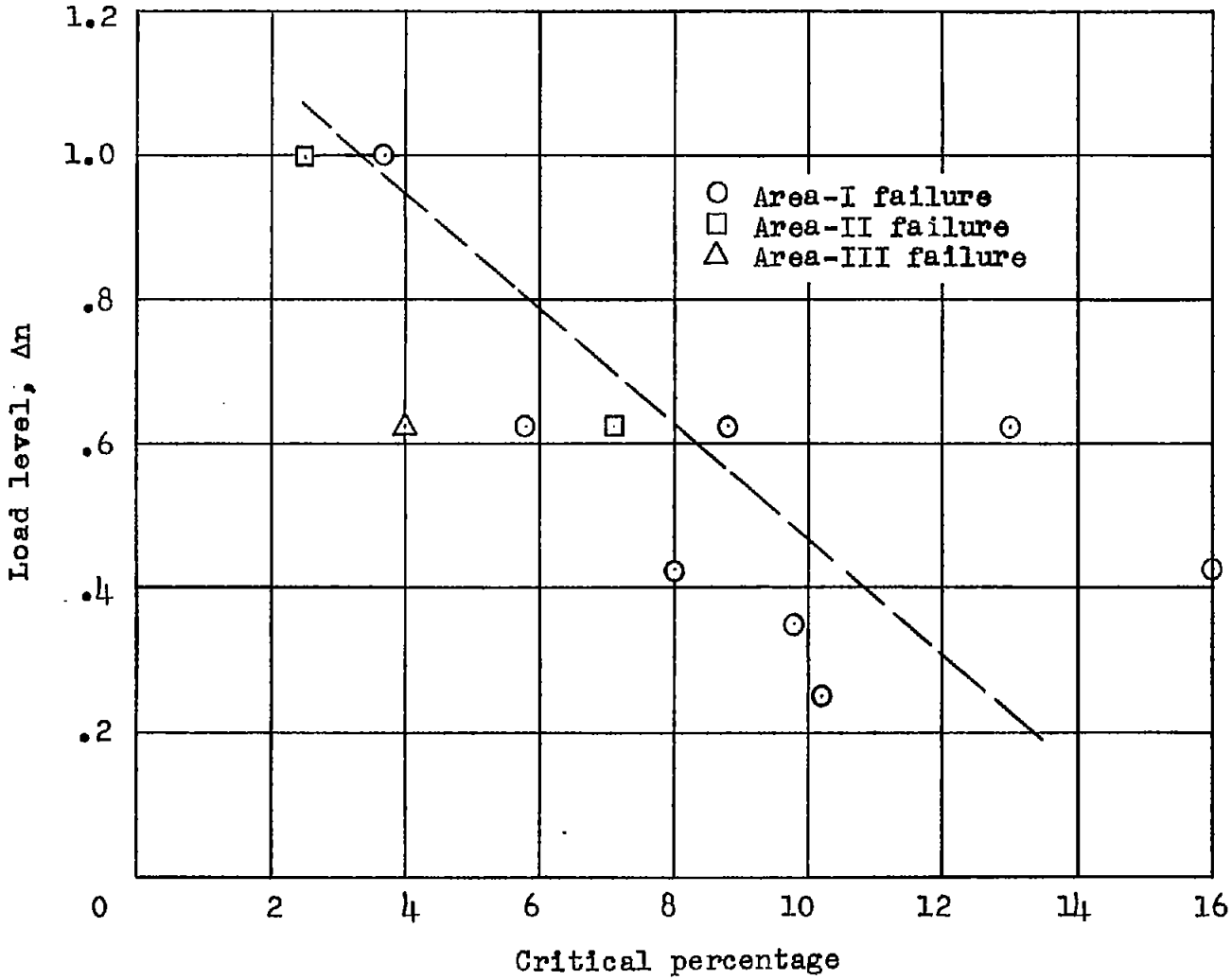

Figure 7.- Tension material failed at critical point.

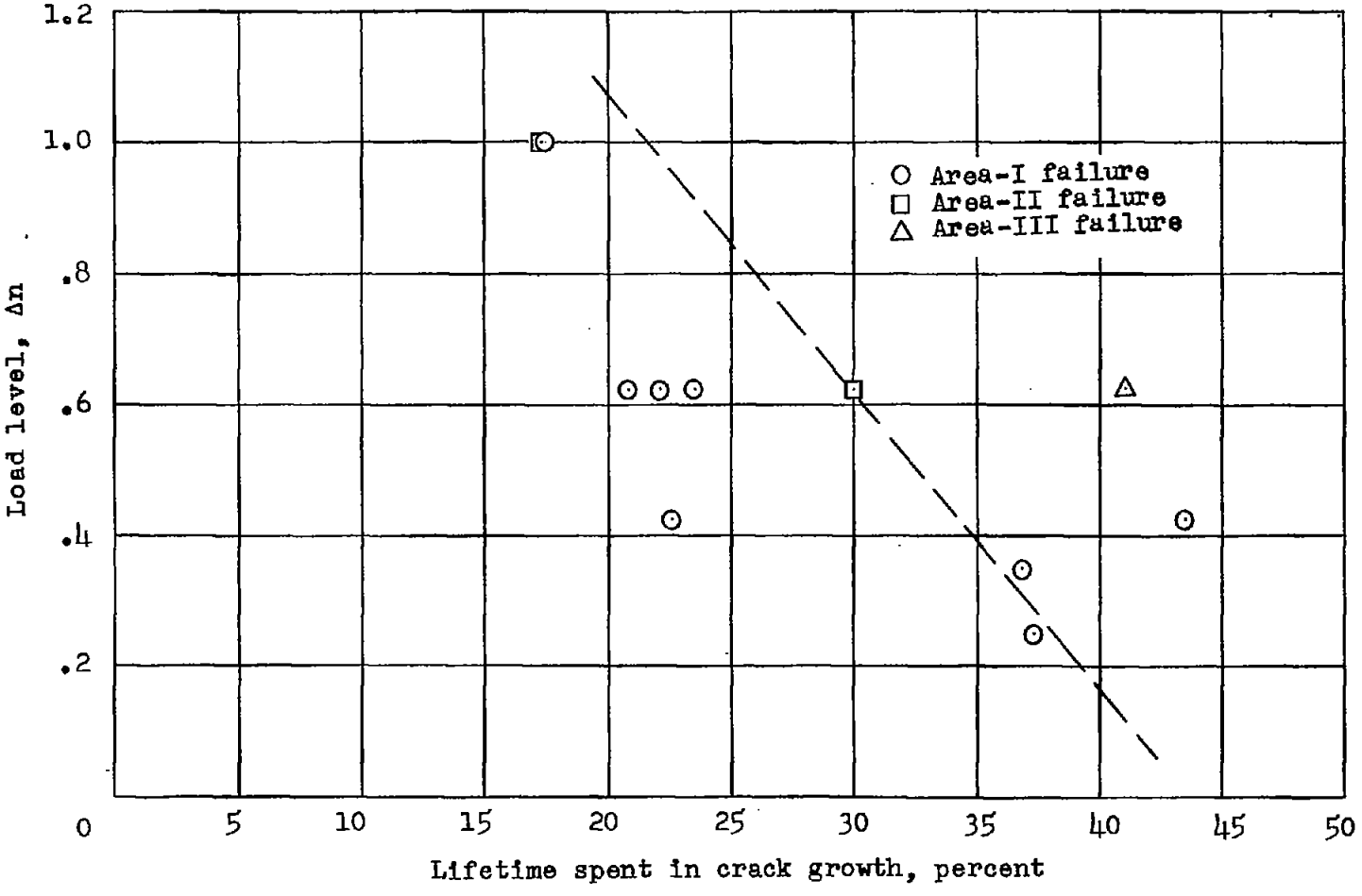

Figure 8.- Lifetime remaining after failure included 1 percent of the tension material.

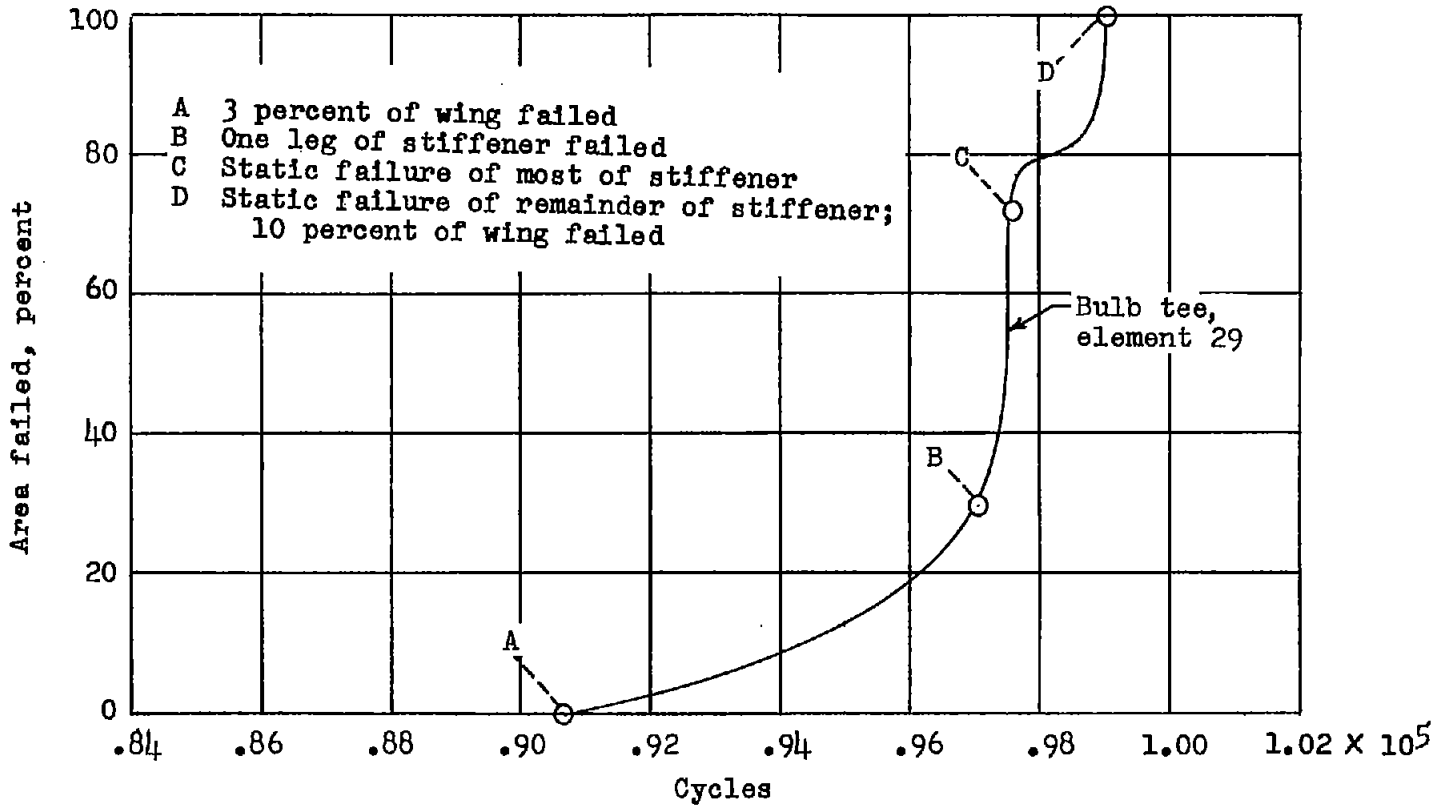

(a) Crack 3; $\Delta n = 1.00$.

Figure 9.- Crack propagation through stiffeners and spar caps.

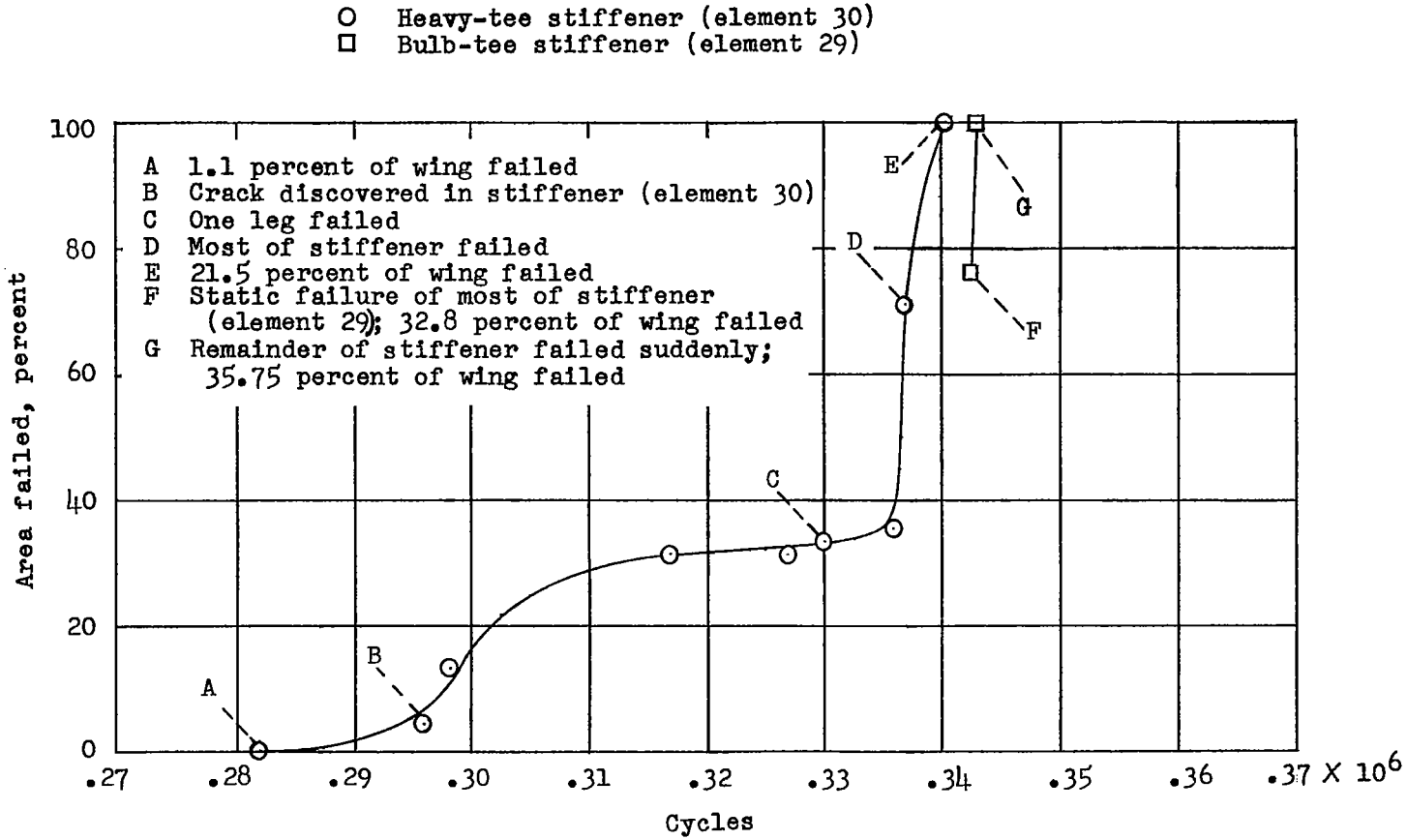

(b) Crack 15; $\Delta n = 0.625$.

Figure 9.- Continued.

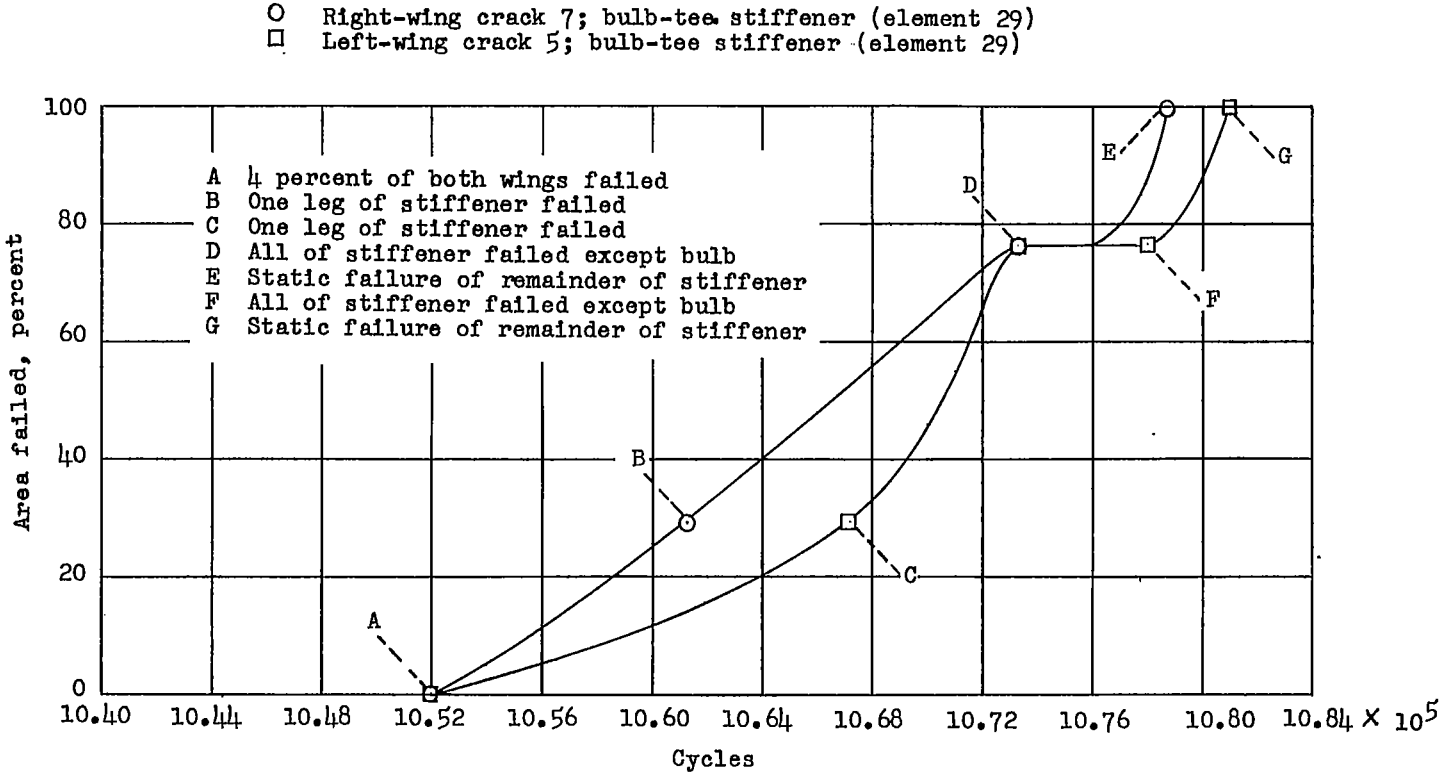

(c) Cracks 5 and 7; $\Delta n = 0.425$.

Figure 9.- Continued.

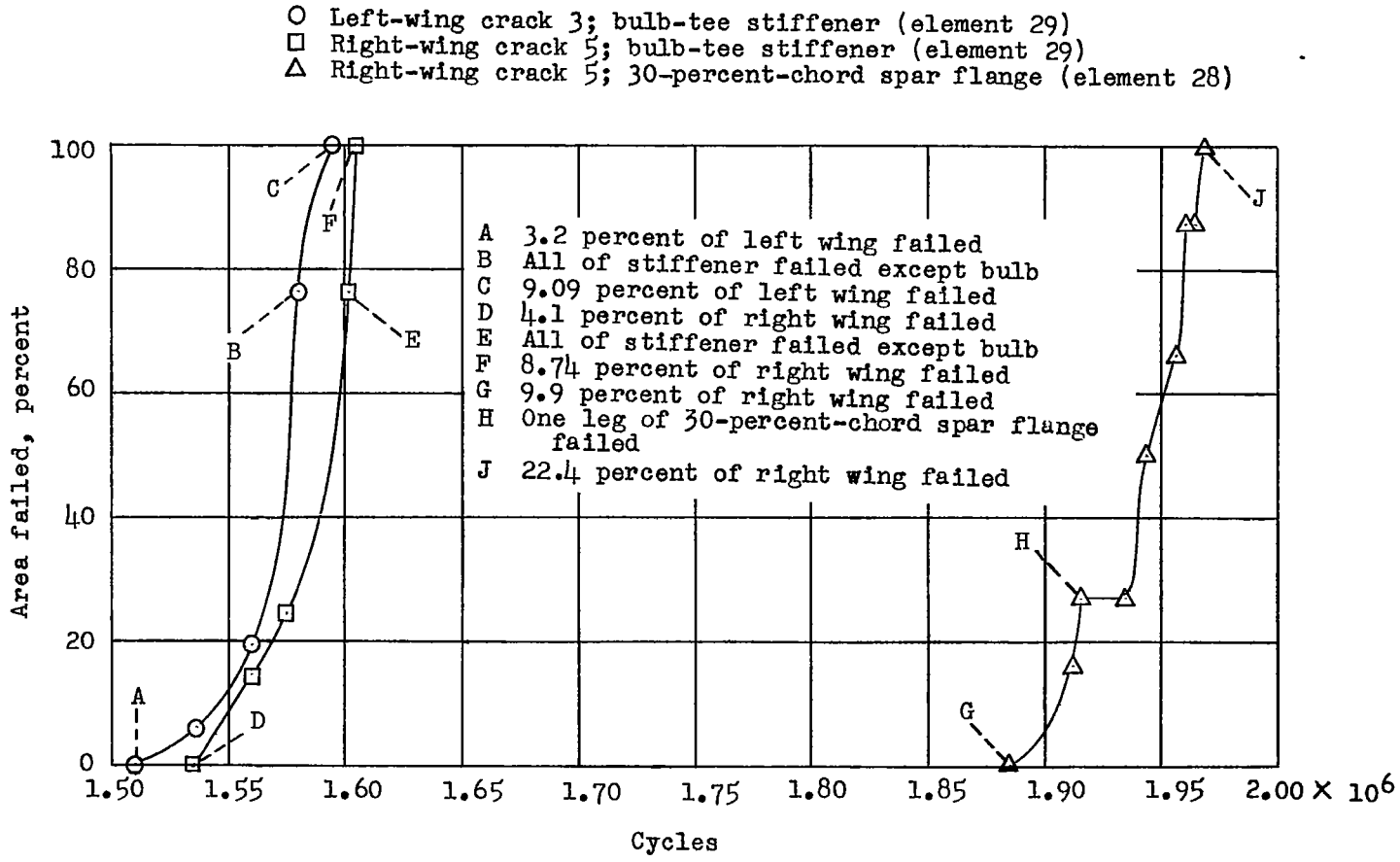

(d) Cracks 3 and 5; $\Delta n = 0.350$.

Figure 9.- Continued.

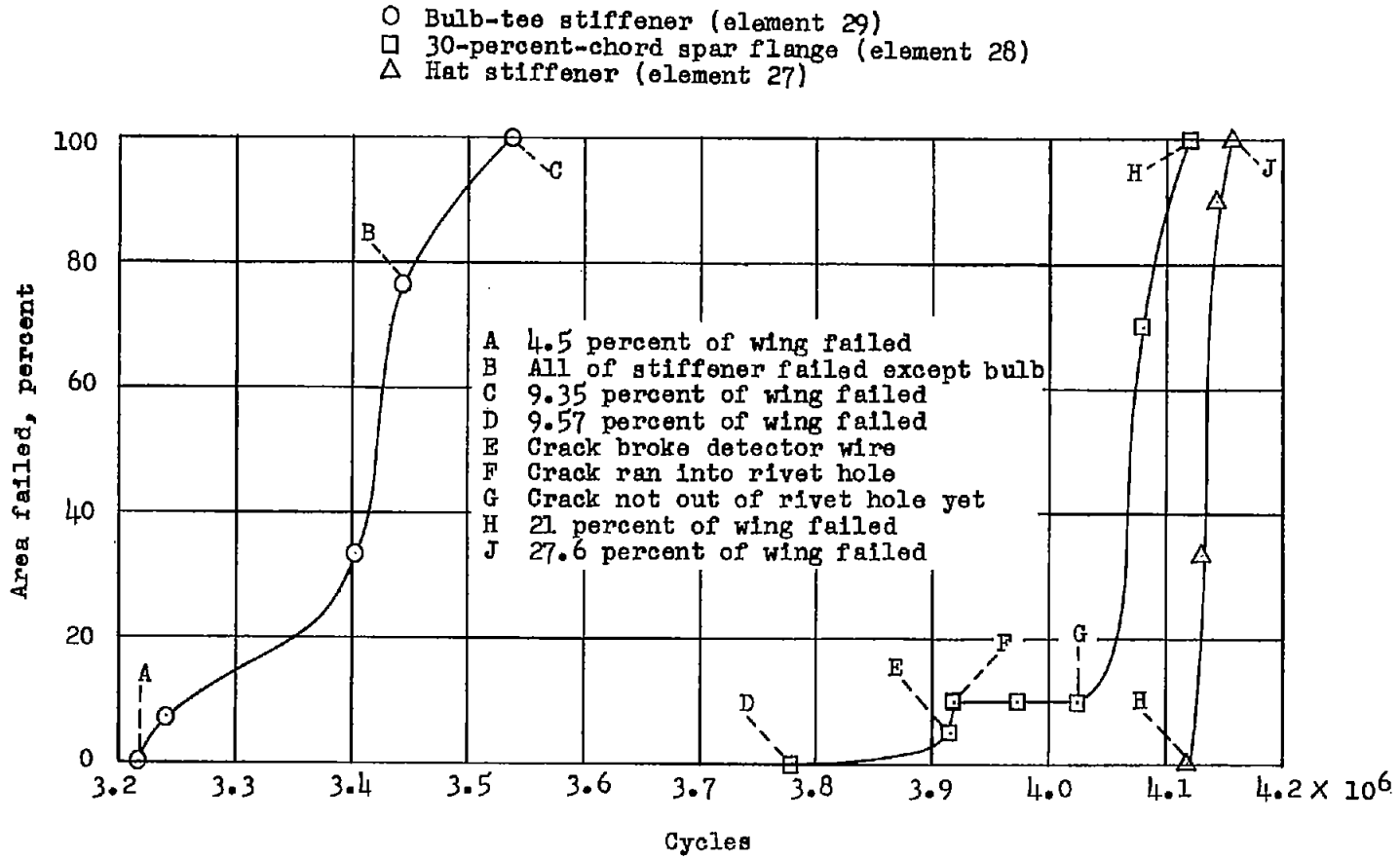

(e) Crack 1; $\Delta n = 0.250$.

Figure 9.- Continued.

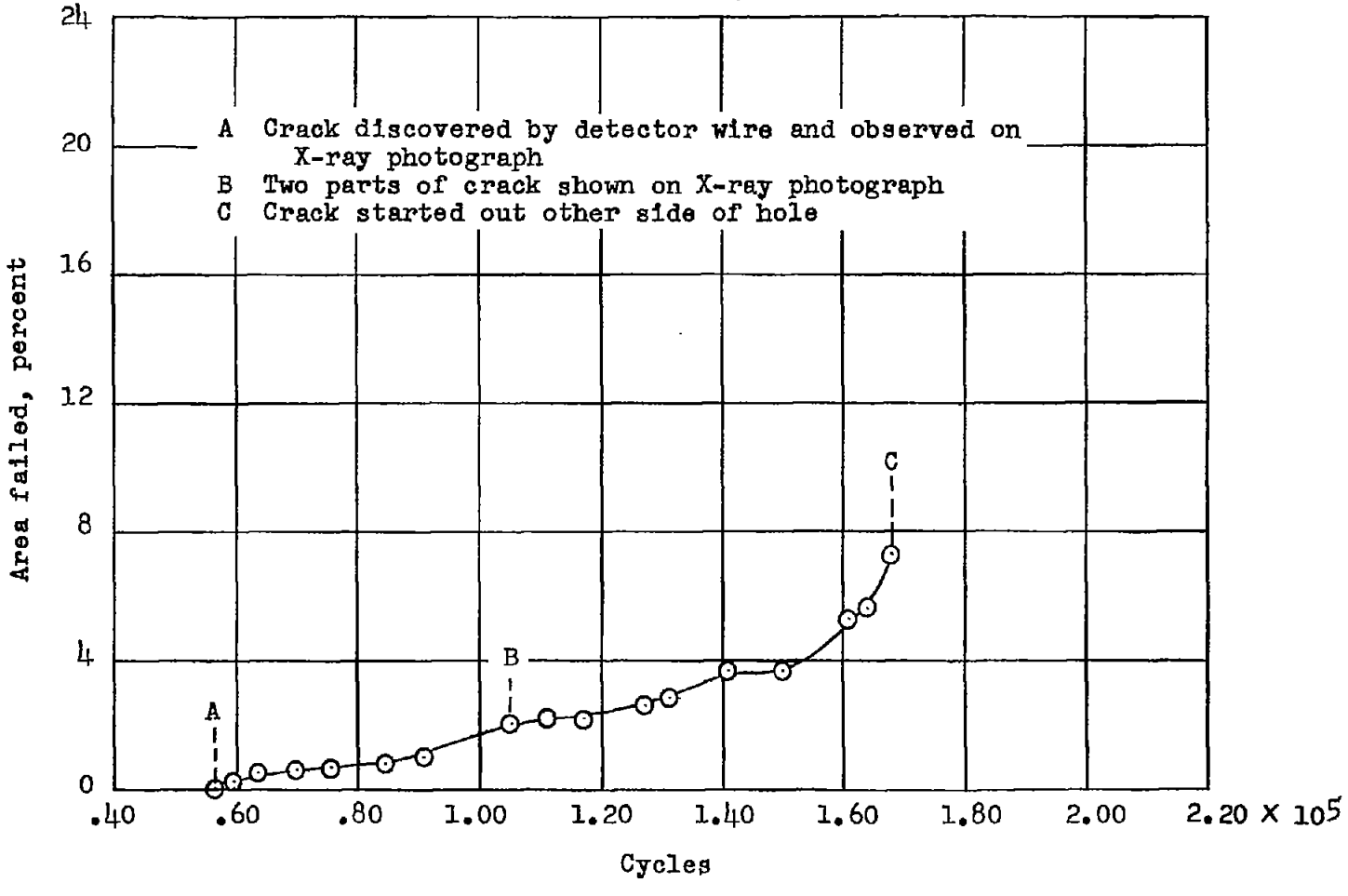

(f) Crack 1; notched spar; $\Delta n = 0.625$.

Figure 9.- Concluded.

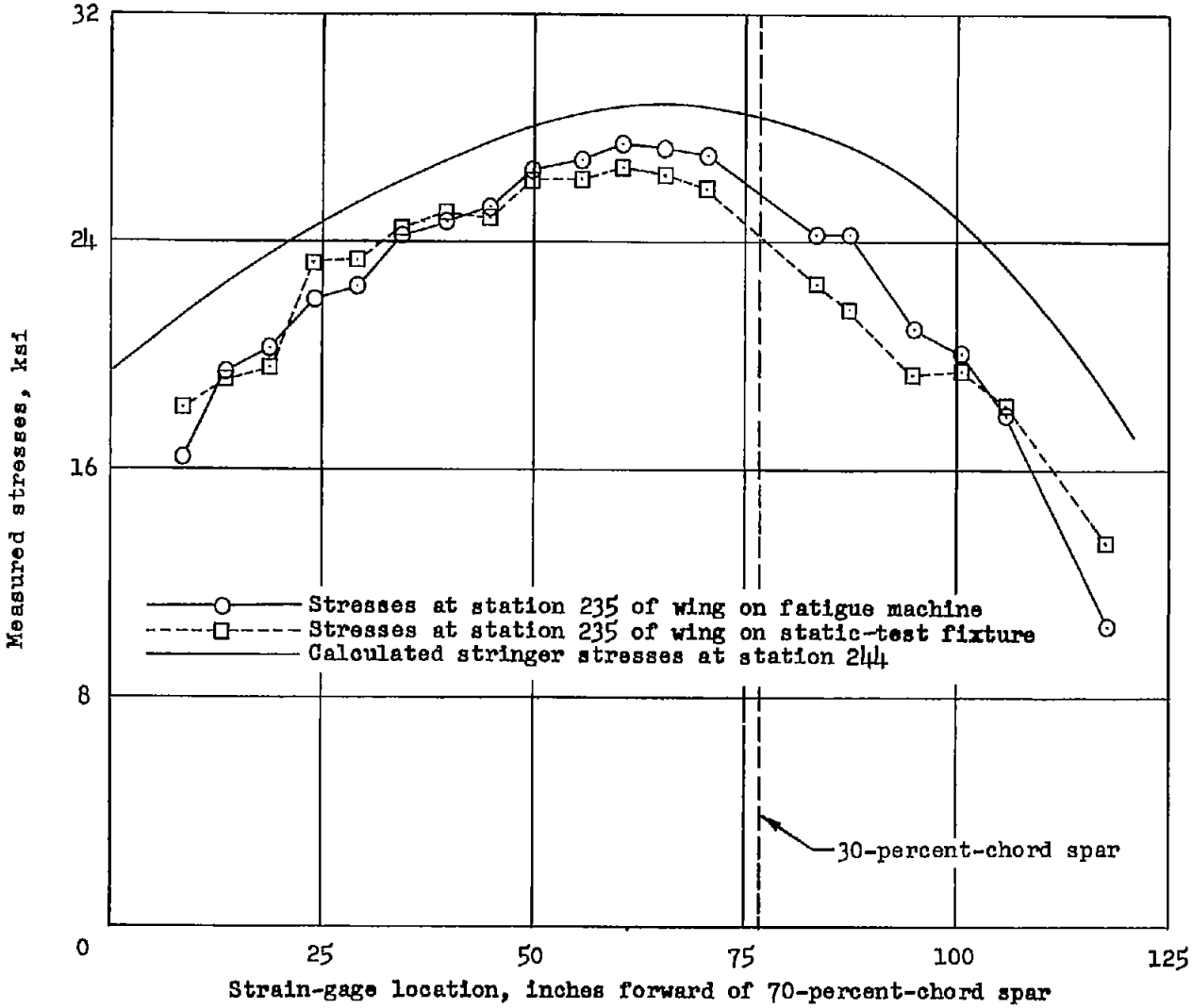

Figure 10.- Chordwise distribution of skin and stringer stresses for 4.0g loading.

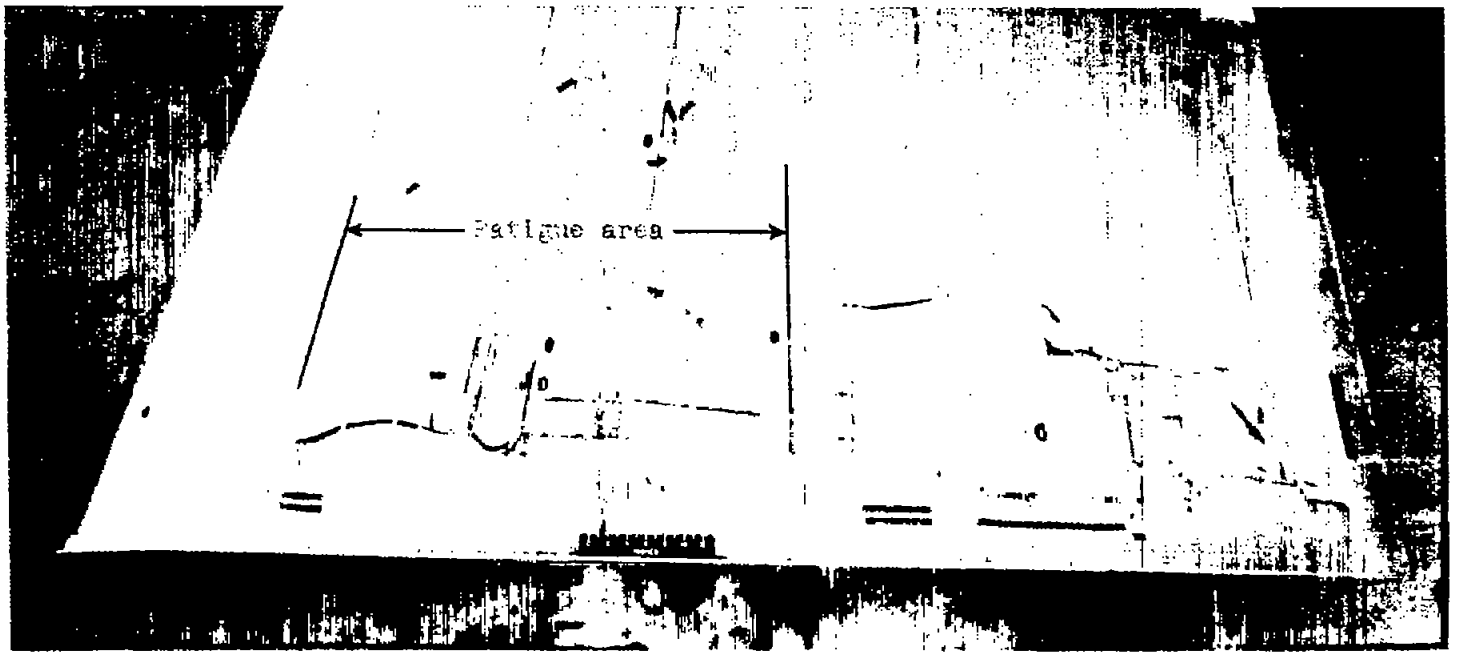

L-89079.1

Figure 11.- Illustration of wing after static test.

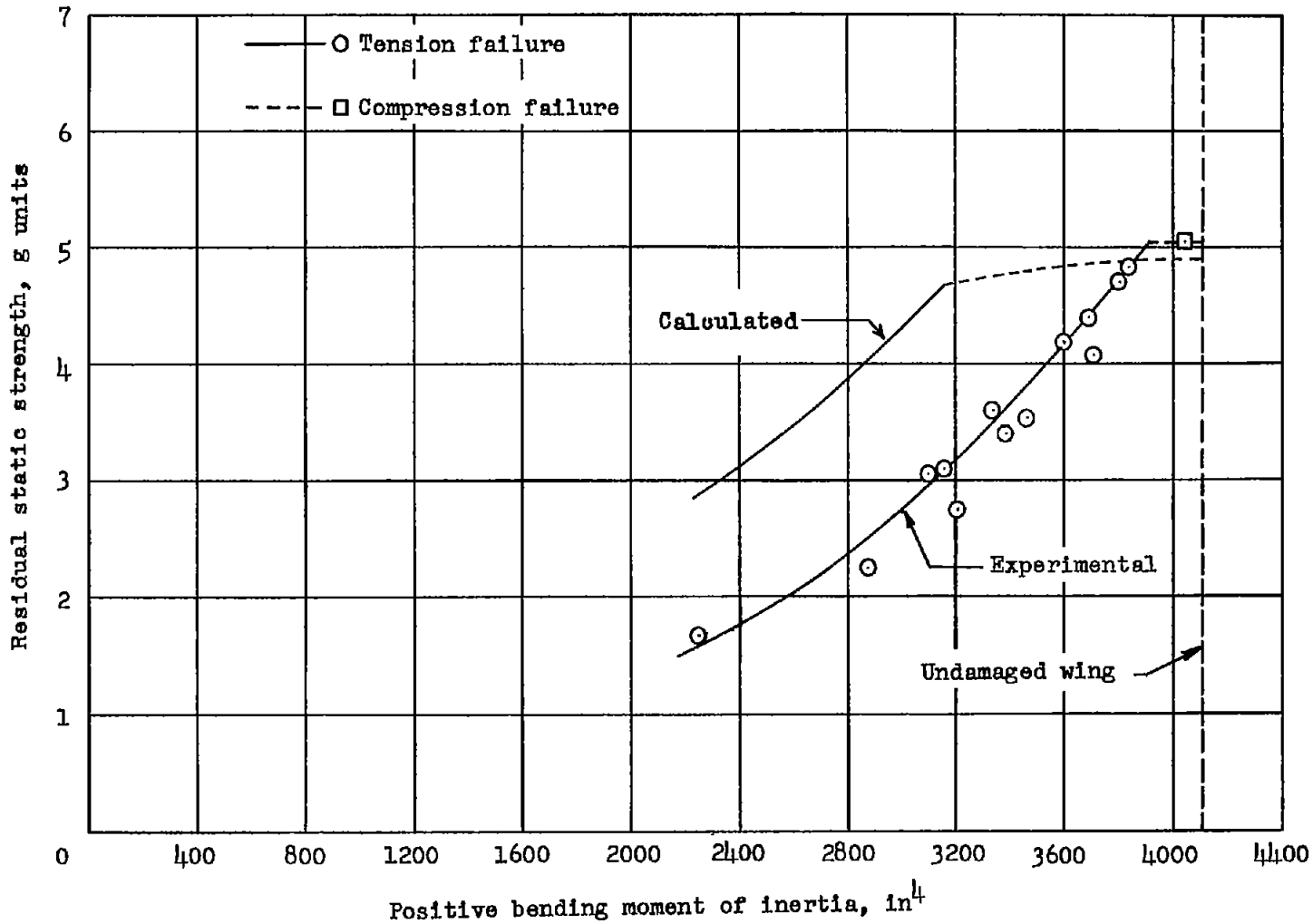

Figure 12.- Residual static strength of C-46 wing in positive bending.

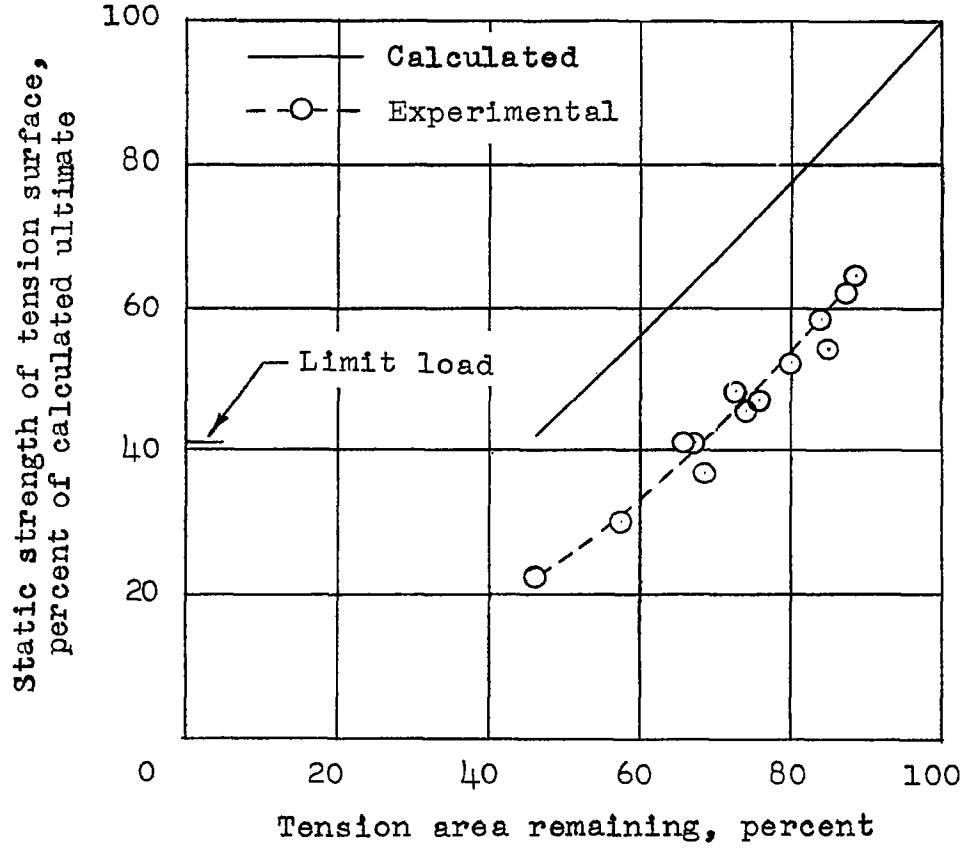

Figure 13.- Residual static strength of tension surface of C-46 wing.

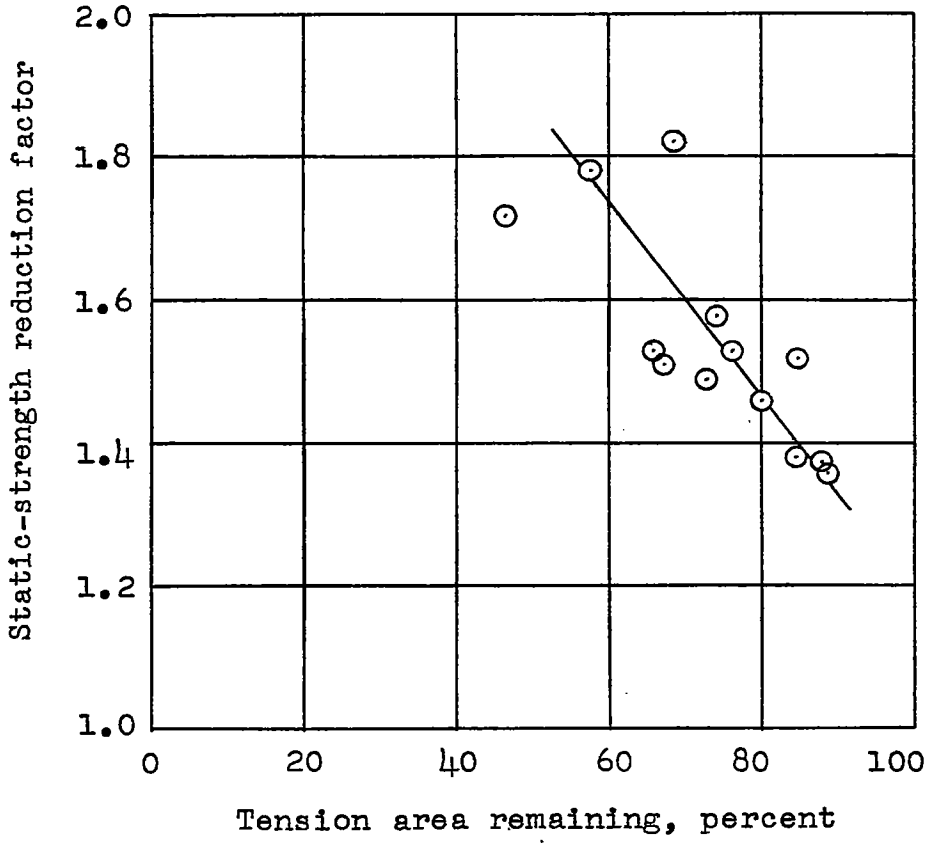

Figure 14.- Static-strength reduction factors for C-46 wing.

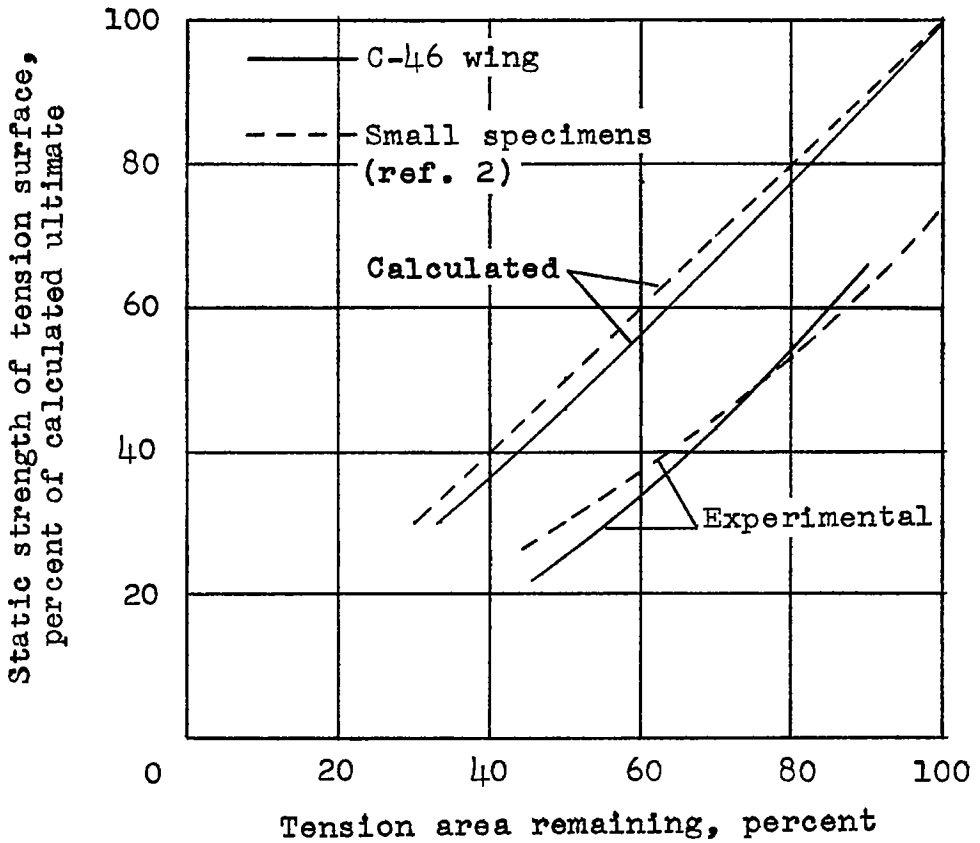

Figure 15.- Comparison of residual static strengths of C-46 wing and small specimens.

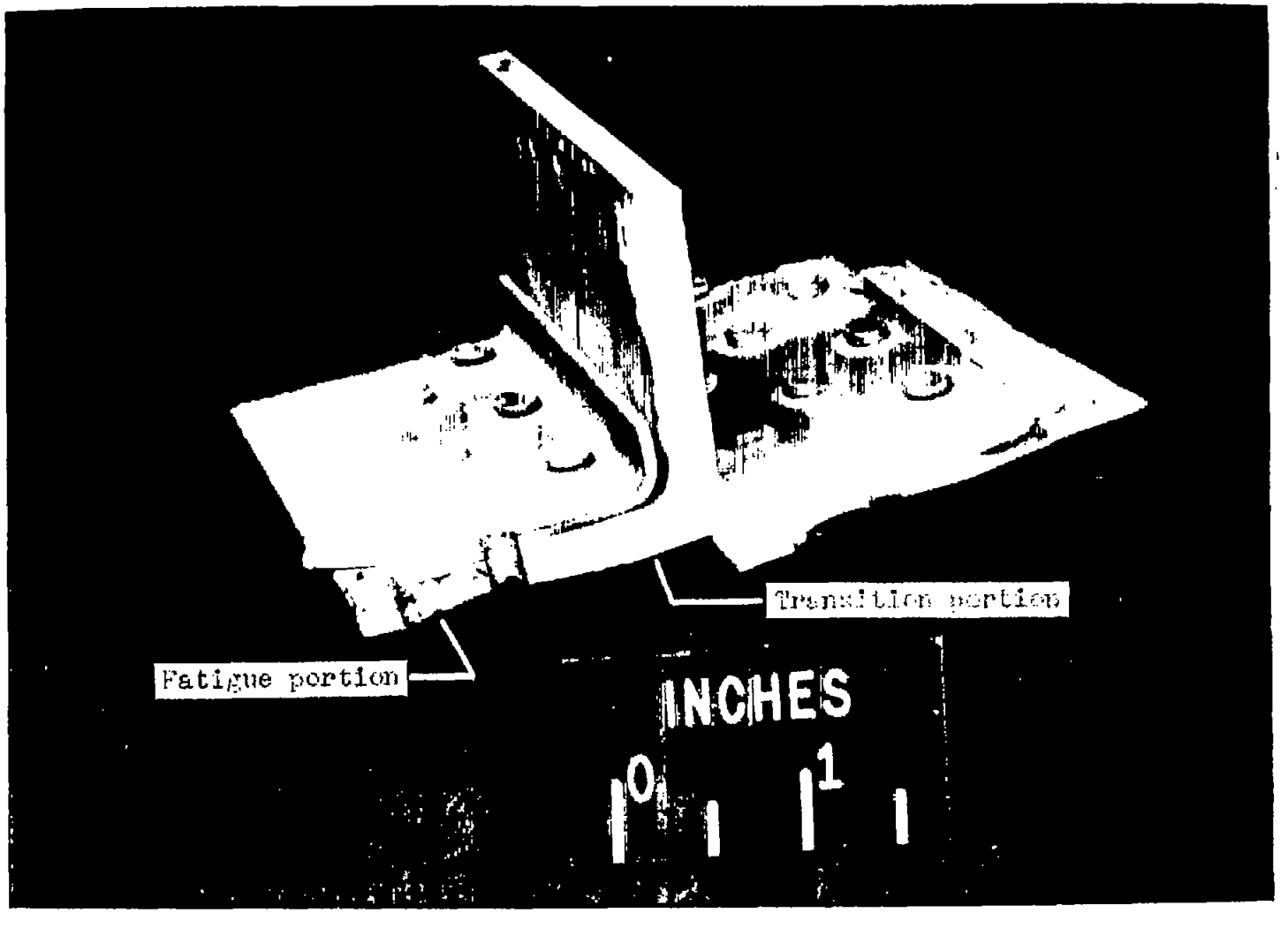

L-90899.1

(a) Failure starting as fatigue type and changing to transition type.

Figure 16.- Typical fractured surface.

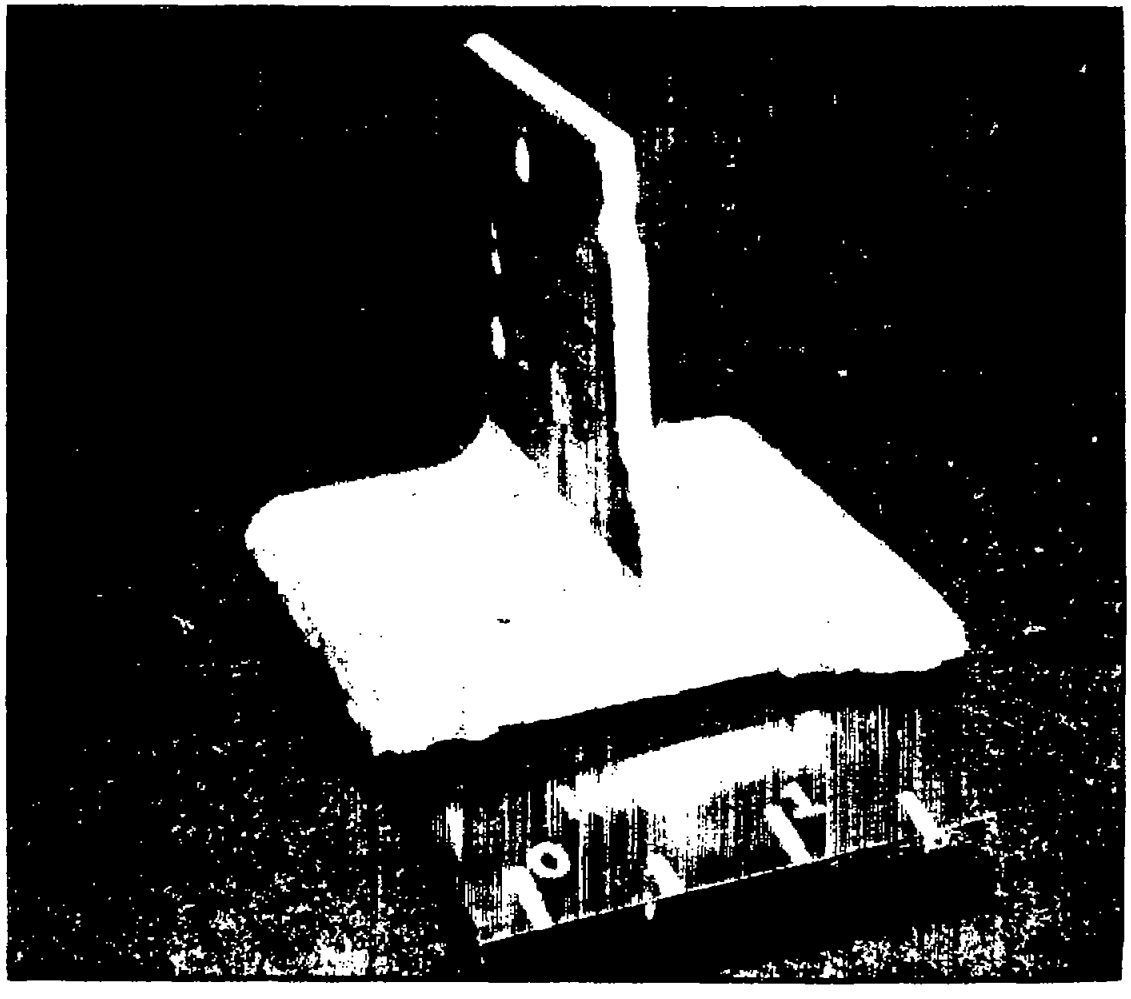

L-90897

(b) Transition type failure.

Figure 16.- Continued.

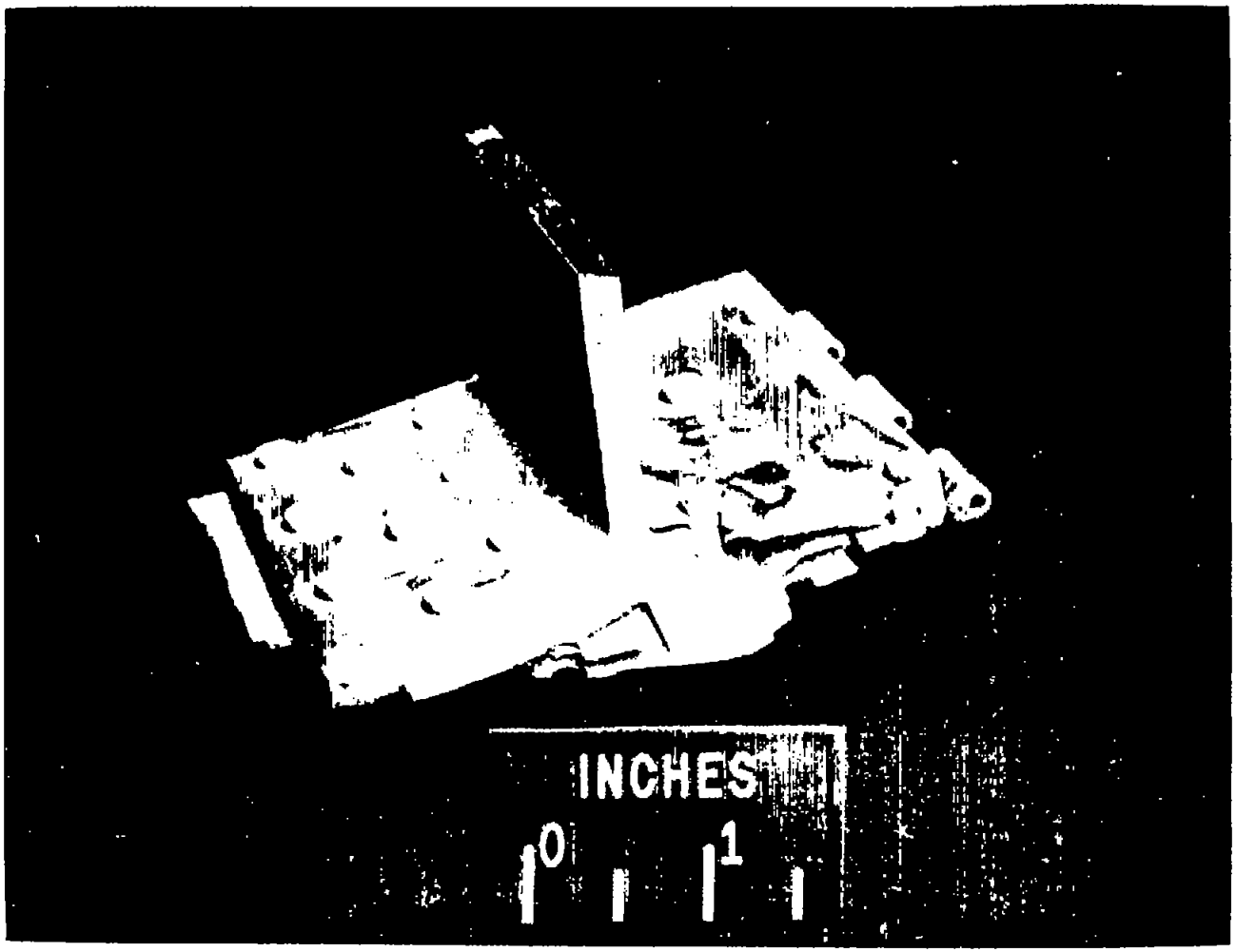

L-90901

(c) Static type failure.

Figure 16.- Concluded.